hydrology

MDPI

*Article*

# Spatio-Temporal Evaluation of Hydrological Pattern Changes Under Climatic and Anthropogenic Stress in an Endorheic Basin: Coupled SWAT-MODFLOW Analysis of the Lake Cuitzeo Basin

**Alejandra Correa-González [1], Joel Hernández-Bedolla [2], Mario Alberto Hernández-Hernández [3,*], Sonia Tatiana Sánchez-Quispe [2], Marco Antonio Martínez-Cinco [1] and Constantino Domínguez Sánchez [2]**

[1] Department of Chemical Engineering, Universidad Michoacana de San Nicolás de Hidalgo, Morelia 58190, Mexico; alejandra.correa@umich.mx (A.C.-G.); marco.martinez@umich.mx (M.A.M.-C.)
[2] Faculty of Civil Engineering, Universidad Michoacana de San Nicolás de Hidalgo, Morelia 58190, Mexico; joel.hernandez@umich.mx (J.H.-B.); quispe@umich.mx (S.T.S.-Q.); dsanchez@umich.mx (C.D.S.)
[3] Natural Resources Department, Geophysics Institute, National Autonomous University of Mexico, Coyoacan, Mexico City 04510, Mexico
* Correspondence: malbher@igeofisica.unam.mx

**Abstract**

In recent years, human activities have impacted surface water and groundwater and their interactions with natural water bodies. Lake Cuitzeo is one of Mexico's most important water bodies but has significantly reduced its flooded area in recent years. Previous studies did not explicitly evaluate the combined effects of hydrological variables on lake dynamics, limiting the understanding of how basin-scale processes influence lake-level. The objective of this study is to evaluate the change in spatio-temporal patterns of hydrological variables under climatic and anthropogenic stress in the Lake Cuitzeo endorheic basin. The proposed methodology uses the SWAT model to analyze at the basin scale, land use and land cover changes, and trends in precipitation and their effect on hydrological processes. Consequently, groundwater flow interactions were assessed for the first time for the Cuitzeo Lake Basin using an automatically coupled SWAT-MODFLOW (v3, 2019), despite limited observational data. A statistically significant change in mean precipitation was detected beginning in 2015, with a decrease of 10.22% compared to the 1973–2014 mean. Land use and land cover changes between 1997 and 2013 resulted in a 26.20% increase in surface runoff. In contrast, estimated evapotranspiration decreased by 1.77%, potentially associated with the reduction in forest cover. As a combined effect of decreased precipitation and land use and land cover change, groundwater percolation declined by 6.34%. Overall, the combined effects of climatic variables and anthropogenic activities have altered lake–aquifer interaction.

**Keywords:** hydrological processes; surface water–groundwater interactions; water bodies; mathematical modeling

Check for updates

Academic Editors: Kristine Walraevens, Alemu Yenehun and Adugnaw Birhanu

Received: 4 December 2025
Revised: 11 January 2026
Accepted: 17 January 2026
Published: 21 January 2026

**Copyright:** © 2026 by the authors. Licensee MDPI, Basel, Switzerland. This article is an open access article distributed under the terms and conditions of the Creative Commons Attribution (CC BY) license.

## 1. Introduction

In recent years, water resources have been negatively affected in both quantity and quality, encompassing rivers, lakes, and groundwater. The primary drivers of these adverse changes are anthropogenic activities [1–3]. Key factors stemming from human actions include the growth of urban centers, which increases the demand for drinking water

and food. This demand leads to the expansion of agricultural areas that consume large amounts of water and fertilizers. Consequently, these activities promote changes in land use and land cover (LULC). Additionally, climate change and deforestation contribute to extreme weather events. As a result, anthropogenic pressures and climatic variability alter hydrological patterns.

Due to their interactions with both surface water and groundwater (SW-GW) systems, lakes are sensitive to the combined effects of anthropogenic pressures and climatic variability. Consequently, their dynamics are driven by multiple factors, most notably climatic variables (precipitation and temperature), LULC change, sediment transport, and groundwater–surface water interactions [4–7].

As a climatic variable, precipitation exhibits spatial and temporal variability depending on its origin, showing either global or localized patterns [8–10]. Furthermore, precipitation varies annually and monthly, with different statistical characteristics. The annual precipitation series exhibits trend variations that can be categorized into normal, dry, or wet sequences [11–13]. However, changes or anomalies within a time series can affect these statistical characteristics. Consequently, several studies apply graphical and statistical analyses to identify potentially atypical values or change points [14,15].

The lake–aquifer connection is defined by the relationship between the lake's water level and the elevation of the water table, as well as the geohydrological characteristics (GHCs). However, assessing the water table in the aquifer is challenging, as it is closely linked to calculating percolation and recharge, variables that have the highest level of uncertainty in quantification [16,17]. Moreover, research indicates that the recharge entering the aquifer can be delayed by days, months, or even years, depending on the soil properties, geological composition, and the depth of the water table [18,19].

In recent years, hydrological models have been widely used as tools to assess the effects of climatic and anthropogenic stresses on hydrological patterns, particularly LULC change and climate change [20–24]. These models provide insights into the relationship between soil variables (e.g., slope, LULC, and soil type) and climatic variables (e.g., precipitation and temperature) for estimating water percolating into the unsaturated zone and quantifying surface runoff. Therefore, several studies have used hydrological models to estimate percolation and groundwater recharge to be used as input information for groundwater flow models [25,26], emphasizing the importance of the basin as a fundamental unit for water resource management [27,28].

This manual coupling of models (a hydrological and a groundwater flow model) has the main advantage of providing a spatially and temporally distributed representation of recharge, calculated from precipitation, to the groundwater model. However, these approaches assume no interactions between groundwater flow and rivers or lakes [29]. Nevertheless, hydrological processes in endorheic basins are inherently more complex due to their closed drainage conditions and interactions between SW-GW [30–33]. Consequently, integrated modeling approaches have been presented frequently in recent years, as they allow establishing key relationships between surface water and groundwater (SW-GW) interactions, such as spatiotemporal recharge processes, bidirectional stream–aquifer exchanges, groundwater contributions to baseflow, and the influence of groundwater levels on surface hydrological responses [34–38].

The SWAT-MODFLOW model (v3, 2019) [39] enables evaluation of SW-GW interactions through a coupled hydrological system. This coupled model combines the SWAT model [40], a widely used, basin-scale, physically based hydrological model [41–43], with the MODFLOW-NWT model (v.1.3.0, 2022) [44], which is a prominent groundwater flow model that has undergone multiple versions since its creation in 1988 [45]. The two models interact by using percolation data calculated from SWAT, which is linked to each cell in

MODFLOW as input data. Additionally, the exchange fluxes between cells defined as streams can be estimated.

Lake Cuitzeo (LC), the second-largest water body in Mexico, is located in the central-western region of the country. It is a shallow water body that regionally collects the discharges from the basin and the aquifer, playing a critical role in environmental services in the area. Mendoza et al. [46] reported that from 1975 to 2000, LC's area decreased by 15%, falling from 346 to 300 km$^2$. However, in recent years, the lake has reduced its flooded area and experienced lower water levels [47]. Research on the LC has focused on climatic variables and LULC change within the watershed [46,48,49]. In 2023, Correa-González et al. conducted a comprehensive analysis of the SW-GW system in Lake Cuitzeo Basin (LCB) through a manual coupling of SWAT-MODFLOW, calculating a groundwater recharge of 182 hm$^3$ per year. However, these studies did not explicitly evaluate the combined effects of SW-GW hydrological variables on lake dynamics, limiting the understanding of how basin-scale processes influence lake-level. For this reason, proposes a methodology for endorheic basins based on the spatio-temporal analysis of surface and subsurface hydrological variables to evaluate changes in hydrological patterns under climatic variability and anthropogenic pressures. The approach aims to identify the main basin-scale processes controlling lake storage dynamics, particularly under data-scarce conditions. The methodology proposes an automatically coupled SWAT-MODFLOW at the basin–aquifer scale to analyze how precipitation and LULC change affect hydrological processes (evapotranspiration, surface runoff, percolation, groundwater recharge, and groundwater flow). This study also evaluates, for the first time, the connections between the lake and the groundwater level despite limited data. This approach provides a more robust evaluation of hydrological pattern changes and contributes to identifying the factors that influence the decline in LC.

## 2. Materials and Methods

### *2.1. Study Area*

The LCB is an endorheic basin covering an area of 4000 km$^2$. The maximum flooded area is 353.95 km$^2$, which accounts for 8.98% of the total basin area. According to CONAGUA [50], the mean annual precipitation is 797 mm, and the average temperature is 17.4 °C. The highest surface runoff in the basin occurs from southwest to northeast, flowing towards LC, with the mainstream being the Grande River of Morelia. Elevations in the area exceed 3000 m above sea level (masl), while the plains near LC have elevations around 1830 masl (Figure 1). The predominant LULC in the basin is agriculture, with irrigated farming concentrated in the plains near the lake and seasonal agriculture distributed throughout the region.

The LCB recharges the Morelia-Queréndaro aquifer (MQA), which has a surface area of 3507 km$^2$. There are approximately 963 extraction wells and 23 springs discharging within the MQA. The average annual water extraction from the aquifer is 160.1 million cubic meters, primarily for urban and agricultural purposes [51].

The MQA is characterized by its heterogeneity and anisotropy, predominantly functioning as an unconfined aquifer with localized semi-confined conditions attributed to clay accumulations near LC. The area is dominated by extrusive igneous rocks found in the higher altitude zones, with basaltic materials comprising 34.15%, tuff 16.82%, and andesite 7.41%. In the plains near the lake, lacustrine and alluvial deposits are predominant, representing 9.02% and 8.13%, respectively. Breccia, volcaniclastic material, rhyolite, dacite, siltstone, and conglomerate are also present, each making up less than 5% of the area (Figure 2).

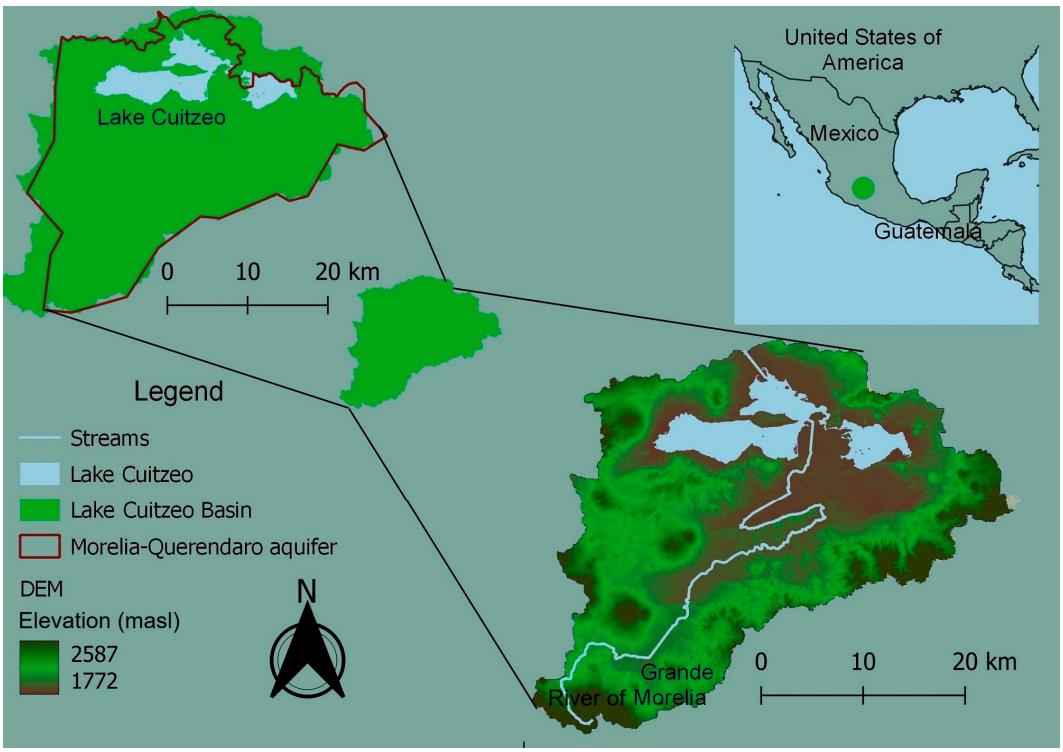



**Figure 1.** Location of the Lake Cuitzeo Basin and the Morelia-Queréndaro aquifer.

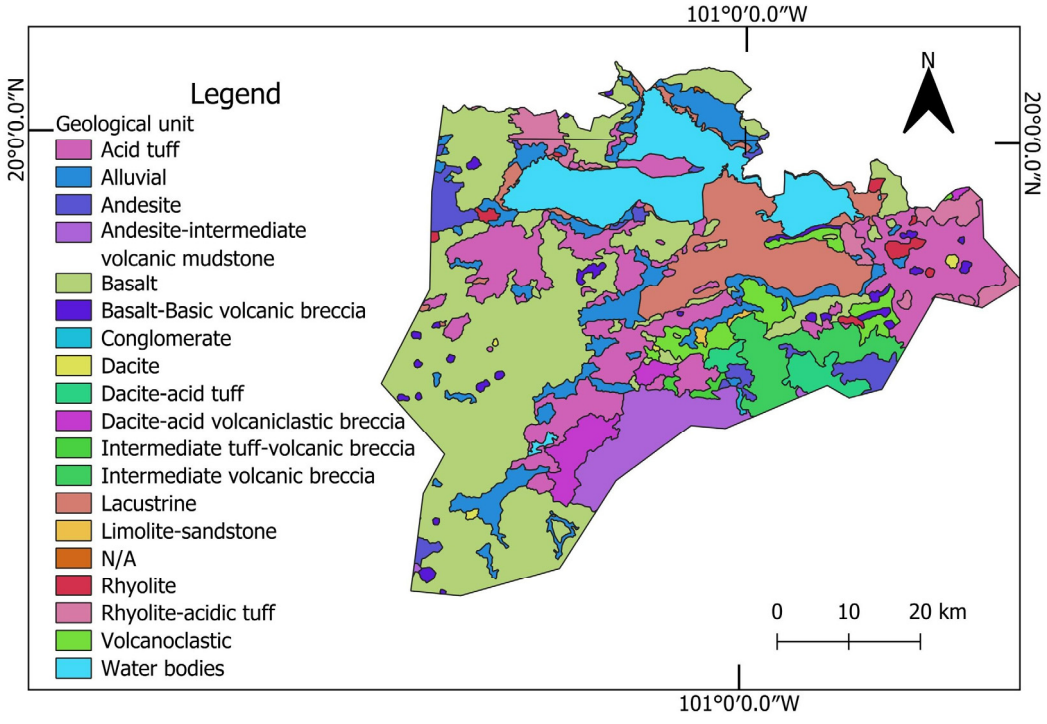



**Figure 2.** Geology of the Morelia-Queréndaro aquifer.

### *2.2. Methodology*

This study presents a methodology for evaluating changes in hydrological patterns in the LCB using coupled SWAT-MODFLOW (v3, 2019) modeling (Figure 3). The analysis focuses on monthly hydrological variables at a basin scale, including precipitation, surface runoff, evapotranspiration, percolation, recharge, and groundwater flow. First, the SWAT model (v2012) is used to model and calibrate two periods of georeferenced LULC data

to evaluate LULC changes. Basin-scale precipitation estimated by SWAT is examined to identify and validate change points and trends within the time series using the cumulative sum (CUSUM) test and the Mann–Kendall (M-K) test to assess the statistical significance of any identified trends. Once change points are detected, the annual precipitation series is visually analyzed for potential anomalies, and Student's *t*-test is employed to determine whether the mean differences between the identified periods are statistically significant. This integrated analysis allows assessing how LULC changes, and precipitation jointly influence surface runoff, evapotranspiration, and percolation. In the second stage, the MODFLOW-NWT (v.1.3.0, 2022) groundwater flow model is implemented through Model Muse [52]. Subsequently, the groundwater model is integrated and calibrated into the coupled SWAT-MODFLOW model.

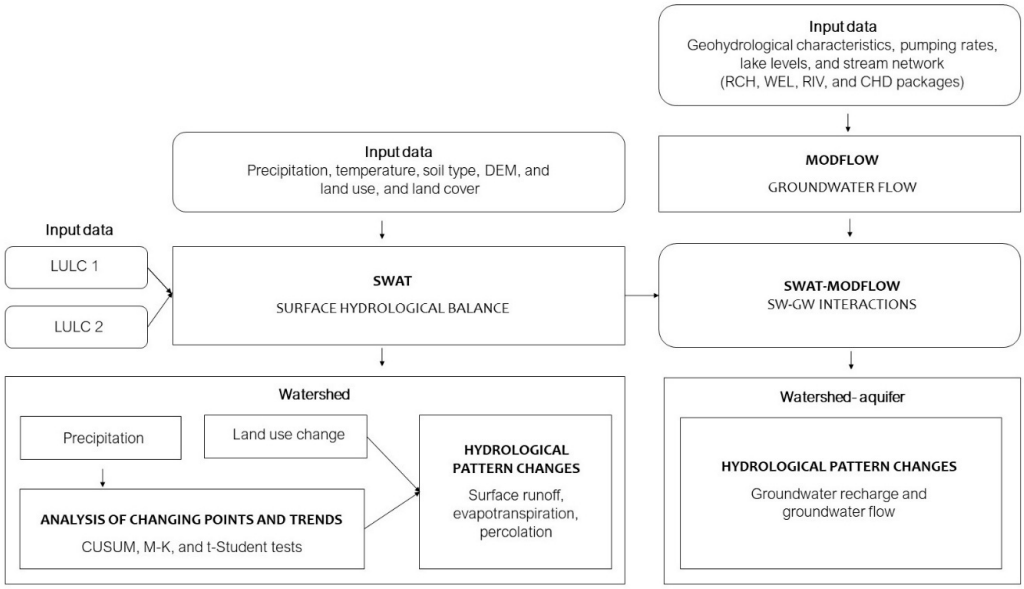



**Figure 3.** Methodology for the analysis of hydrological pattern changes in basin-aquifer interactions.

#### 2.2.1. SWAT Model

The SWAT model is a physically based, sub-aggregated hydrological model that calculates the daily surface water balance through Hydrological Response Units (HRUs). The water balance is determined using the following equation [53]:

$$SW_t = SW_O + \sum_{i=1}^{t}\left(R_{day} - Q_{surf} - E_a - W_{seep} - Q_{gw}\right) \quad (1)$$

where $SW_t$ is the final soil water content (mm), $SW_0$ is the initial soil water content on day $i$ (mm), $t$ is the time (days), $R_{day}$ is the amount of precipitation on day $i$ (mm), $Q_{surf}$ is the amount of surface runoff on day $i$ (mm), $E_a$ is the amount of evapotranspiration on day $i$ (mm), $W_{seep}$ is the amount of water entering the vadose zone of the soil profile on day $i$ (mm), and $Q_{gw}$ is the amount of return flow on day $i$ (mm).

#### 2.2.2. MODFLOW Model

MODFLOW-NWT uses a Newton-based linearization approach to simulate three-dimensional groundwater flow based on the solution variables of MODFLOW-2005. The following equation illustrates its symbolic form:

$$J\left(h^{n-1}\right)h^n = R^{n-1} + J\left(h^{n-1}\right)h^{n-1} \quad (2)$$

where $n$ and $n-1$ are the nonlinear iteration counters for the current and previous iterations, respectively, $J$ is the Jacobian matrix, $h^{n-1}$ is the groundwater height at iterations $n$ and $n-1$, and $R$ is the residual vector that represents the cell-by-cell errors in the water balance. $R$ is calculated by adding all the inputs and outputs of each cell.

#### 2.2.3. SWAT-MODFLOW Model

The SWAT-MODFLOW model integrates the SWAT 2012 model with MODFLOW-NWT [44]. This integration between the two models is accomplished by disaggregating HRUs into individual polygons. These disaggregated HRUs (dHRUs) intersect with the grid cells of MODFLOW-NWT, allowing for the exchange of variables between SWAT and MODFLOW. The interactions between groundwater flow and streams are calculated using the river package in MODFLOW.

#### 2.2.4. Cumulative Sum Test

The CUSUM test is a widely used non-parametric sequential graphical method for identifying change points in precipitation series [54,55]. The CUSUM test detects change points by analyzing the cumulative sum of deviation $O_i$-$O_m$, where $O_i$ is the value at index $i$ of the observed series and $O_m$ is the mean of the observed series. An increasing sequence indicates a wet period (above the mean), while a decreasing sequence indicates a dry period (below the mean). A sequence that fluctuates around the mean is considered normal.

#### 2.2.5. Mann–Kendall Test

The M-K test is a non-parametric method used to identify statistically significant trends in climatic and hydrologic time series data [56–58]. The M-K test is calculated as follows:

$$S = \sum_{i=1}^{n=1} \sum_{j=i+1}^{n} sign\left(x_j - x_i\right), sign\left(x_j - x_i\right) = \begin{array}{ll} +1 & \left(x_j - x_i\right) > 0 \\ 0 & \left(x_j - x_i\right) = 0 \\ -1 & \left(x_j - x_i\right) < 0 \end{array} \quad (3)$$

$$Z = \frac{S \pm 1}{Var(S)^{1/2}} \quad (4)$$

$Z$ is used to evaluate the presence of trends. A positive $Z$ value indicates an increasing trend, while a negative $Z$ value suggests a decreasing trend. If $|Z| < 1.96$, there is no statistical evidence of a trend at the 95% confidence level. Additionally, if the $p$-value > 0.05, the null hypothesis ($H_0$), which states that there is no significant trend, is not rejected.

#### 2.2.6. Student's *t*-Test

Student's $t$-test is a parametric test used to determine whether a precipitation time series reveals a statistically significant change between two time periods [59–61].

$$t = \frac{|\overline{x_2} - \overline{x}_2|}{S\sqrt{\frac{1}{n_1} + \frac{1}{n_2}}} \quad (5)$$

$$S = \sqrt{\frac{(n_1 + 1){s_1}^2 + (n_2 - 1){s_2}^2}{n - 2}} \quad (6)$$

where $x_1$ and $x_2$ are the calculated means of the first and second periods, while ${s_1}^2$ and ${s_2}^2$ are the variances for each period. Additionally, $n_1$ and $n_2$ are the number of values in each subseries. The critical values for this test are obtained from Student's $t$-test using $n-2$ degrees of freedom and a significance level of 5%.

2.2.7. Model Calibration

The calibration of the surface hydrological model is based on statistical metrics commonly used in hydrological models [62]. These parameters include the coefficient of determination ($R^2$; Equation (7)), the Nash-Sutcliffe efficiency index ($NSE$; Equation (8)), and percentage bias ($PBIAS$; Equation (9)).

The calibration of the groundwater flow model is performed using the percolation data calculated from the SWAT model. Based on this recharge, the hydrogeological parameters of the groundwater model are adjusted using the mean absolute error ($MAE$; Equation (10)) and root mean square error ($RMSE$; Equation (11)).

$$R^2 = \left( \frac{\sum_{i=1}^{n}(O_i - O_m)(S_i - S_m)}{\sqrt{\sum_{i=1}^{n}(O_i - O_m)^2 (S_i - S_m)^2}} \right)^2 \quad (7)$$

$$\mathrm{NSE} = 1 - \frac{\sum_{i=1}^{n}(O_i - S_i)^2}{\sum_{i=1}^{n}(O_i - O_m)^2} \quad (8)$$

$$PBIAS = \frac{\sum_{i=1}^{n} O_i - S_i}{\sum_{i=1}^{n} O_i} \times 100 \quad (9)$$

$$MAE = \frac{\sum_{i=1}^{n}|O_i - S_i|}{n} \quad (10)$$

$$RMSE = \sqrt{\frac{\sum_{i=1}^{n}(O_i - S_i)^2}{n}} \quad (11)$$

where $O_i$ is the value at index $i$ of the observed series, $O_m$ is the mean of the observed series, $S_i$ is the value at index $i$ of the simulated series, $S_m$ is the mean of the simulated series, and $n$ is the number of values present in the observed and/or simulated series.

*2.3. SWAT Application*

The configuration of the sub-basin model was developed using a digital elevation model (DEM) in raster format with a pixel resolution of 200 m. Georeferenced data on LULC and soil types were incorporated using the same characteristics as the DEM. The modeling period spans from 1973 to 2020, with a monthly time step. A total of two hydrometric stations (HS) and ten climatological stations were utilized (Figure 4a). Streamflow data were obtained from BANDAS [63], while the precipitation and temperature series were extracted from CICLOM [64] and SMN [65]. The distribution of soil types in the watershed is illustrated in Figure 4b. The assessment of LULC change was conducted using georeferenced geographic data from 1997 and 2013. The georeferenced data for the DEM, soil types, and LULCs were sourced from INEGI [66]. The reclassification of LULC was performed according to the database within the SWAT program. The basin includes ten LULCs: agricultural, water, non-forested wetlands, residential, evergreen forest, deciduous forest, mixed forest, grassland range, barren land, and brush range (Figure 4c,d). Based on the DEM, slope, LULC, and soil type, 51 sub-basins were created, resulting in 543 HRUs for 1997 and 505 HRUs for 2013. Evapotranspiration was calculated using the Hargreaves method [67].

*2.4. SWAT-MODFLOW Application*

The characterization and boundary conditions of the aquifer were defined both spatially and temporally. The aquifer was discretized into 2000 × 2000 m cells as a single unconfined layer, with top and bottom elevations based on the DEM and a total thickness of 300 m. The bottom and lateral boundary conditions were set as no-flow boundaries. The

inputs and outputs considered within the aquifer included recharge (RCH), groundwater extraction (WEL), water exchange with rivers (RIV), and constant head boundary condition cells (CHD).

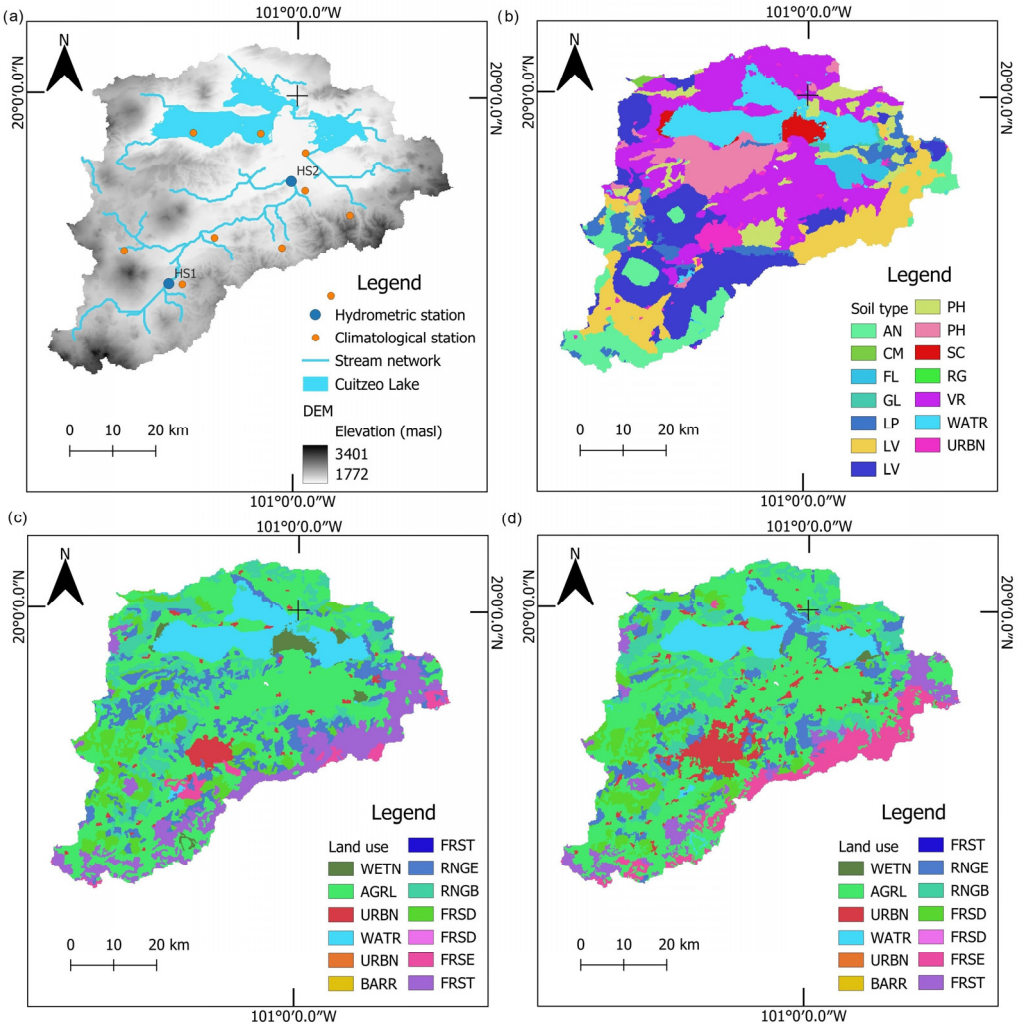



**Figure 4.** (**a**) Digital Elevation Model (DEM) and the locations of hydrometeorological stations; (**b**) soil type; (**c**) land use for 1997; and (**d**) land use for 2013. The categories are as follows: Wetlands-Non-Forested (WETN), Agricultural (AGRL), Residential (URBN), Water (WATR), Range-Grasses (RNGE), Range-Brush (RNGB), Forest-Deciduous (FRSD), Forest-Evergreen (FRSE), Forest-Mixed (FRST), and Barren (BARR).

Figure 5 illustrates the model configuration in SWAT-MODFLOW. Observation points, pumping rates, the stream network, and LC are shown in Figure 5a. The GHCs were proposed according to the aquifer's geology (Figure 5b). The stream network and LC discretization are depicted in Figure 5c. LC was discretized using 92 cells, with elevations assigned based on the DEM, resulting in a mean elevation of 1823.16 masl. The stream network used in MODFLOW was also discretized and generated within SWAT. Groundwater extraction was assumed to be constant over time, with an annual total of 181.07 $hm^3$. The pumping rates for each model cell are provided in Figure A1b in Appendix A.

The coupling of the SW-GW system models was carried out automatically through the SWAT-MODFLOW interface for QGIS [35,68]. The spatial discretization of the recharge is also detailed in Figure A1a in Appendix A. The percolation rate calculated using the SWAT model is 158.94 $hm^3$ per year, and was applied to two zones according to CONAGUA [69]:

Zone 1 is located in the lacustrine plain, while Zone 2 is located in the upper areas of the basin, where the GHCs are characterized by extrusive igneous rocks (Figure 5d).

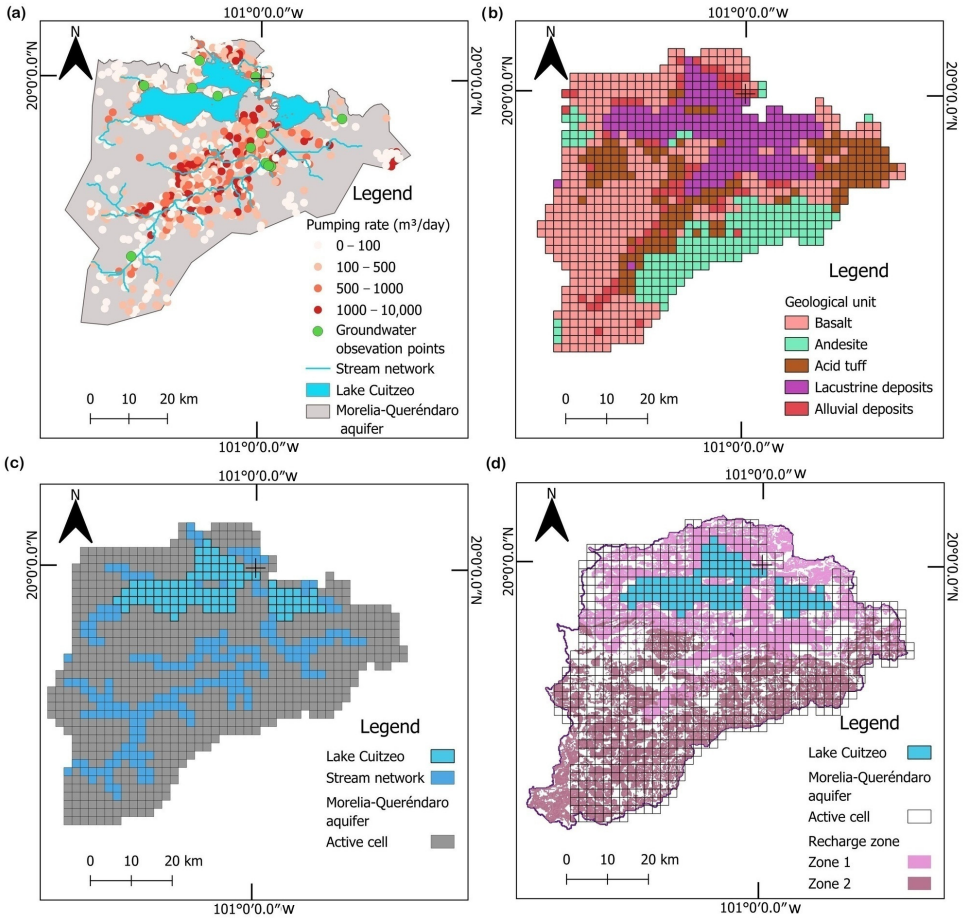



**Figure 5.** Model configuration in SWAT-MODFLOW. (**a**) Groundwater observation points, pumping rates, stream network, and Lake Cuitzeo; (**b**) geology unit discretization; (**c**) stream network and Lake Cuitzeo discretization; and (**d**) recharge zone.

### *2.5. Calibration of Models*

The simulated period was carried out from 1970 to 2020, including a three-year warm-up period from 1970 to 1972. The model was calibrated using the 1997 LULC dataset and validated using the 2013 LULC dataset within the SWAT framework. Consequently, the same set of calibrated parameter values was applied to both LULC scenarios. Table A1 in the Appendix A presents the parameter ranges and calibrated values for each LULC condition. Table 1 presents the adjustment achieved for the two LULC data (1997 and 2013) using SWAT and SWAT-MODFLOW. The calibration in both LULC data utilizes observed data from two HS. At HS1, the observed streamflow measured 2.36 $m^3/s$. However, all three models underestimated this flow, with predicted values of 2.01, 2.11, and 2.05 $m^3/s$. $R^2$ for the three models is approximately 0.57. NSE demonstrates the best fit in the coupled SWAT-MODFLOW model, with a value of 0.55. PBIAS ranges from 5.96 to 14.92. In the case of HS2, the mean stream flow is 4.60 $m^3/s$. In contrast, the three simulations overestimate this flow with predictions of 4.96, 5.02, and 6.20 $m^3/s$. The $R^2$ remains ~0.5 for all three models, and the NSE values range from 0.39 to 0.25. The coupled model exhibits the highest PBIAS at 34.59.

**Table 1.** Comparison of monthly mean streamflow and statistical metrics.

| LULC/Model | Station | Period | Streamflow | | $R^2$ | NSE | PBIAS |
|---|---|---|---|---|---|---|---|
| | | | O.M. [1] $m^3/s$ | S.M. [1] $m^3/s$ | | | |
| LULC 1997/SWAT Calibration | HS1 | 1973–2002 | 2.36 | 2.01 | 0.57 | 0.49 | 14.92 |
| | HS2 | 1973–1984 | 4.60 | 4.96 | 0.49 | 0.39 | −7.73 |
| LULC 2013/SWAT Validation | HS1 | 1973–2002 | 2.36 | 2.11 | 0.57 | 0.25 | 5.96 |
| | HS2 | 1973–1984 | 4.60 | 5.02 | 0.51 | 0.39 | −8.96 |
| LULC 2013/SWAT-MODFLOW | HS1 | 1973–2002 | 2.36 | 2.05 | 0.57 | 0.55 | 12.86 |
| | HS2 | 1973–1984 | 4.60 | 6.20 | 0.49 | 0.25 | −34.59 |

[1] Observed monthly mean (O.M.), simulated monthly mean (S.M.).

Figure 6 compares the streamflow at the HSs used for model calibration in the SWAT-MODFLOW for the 2013 LULC data. HS1 presents a base flow of approximately 0.5 $m^3/s$ during the early years of the observed series, which decreases over time. The simulated streamflow maintains this base flow throughout the modeling period. However, the direct flow is underestimated. In contrast, at HS2, the model overestimates both the base flow and the direct flow.

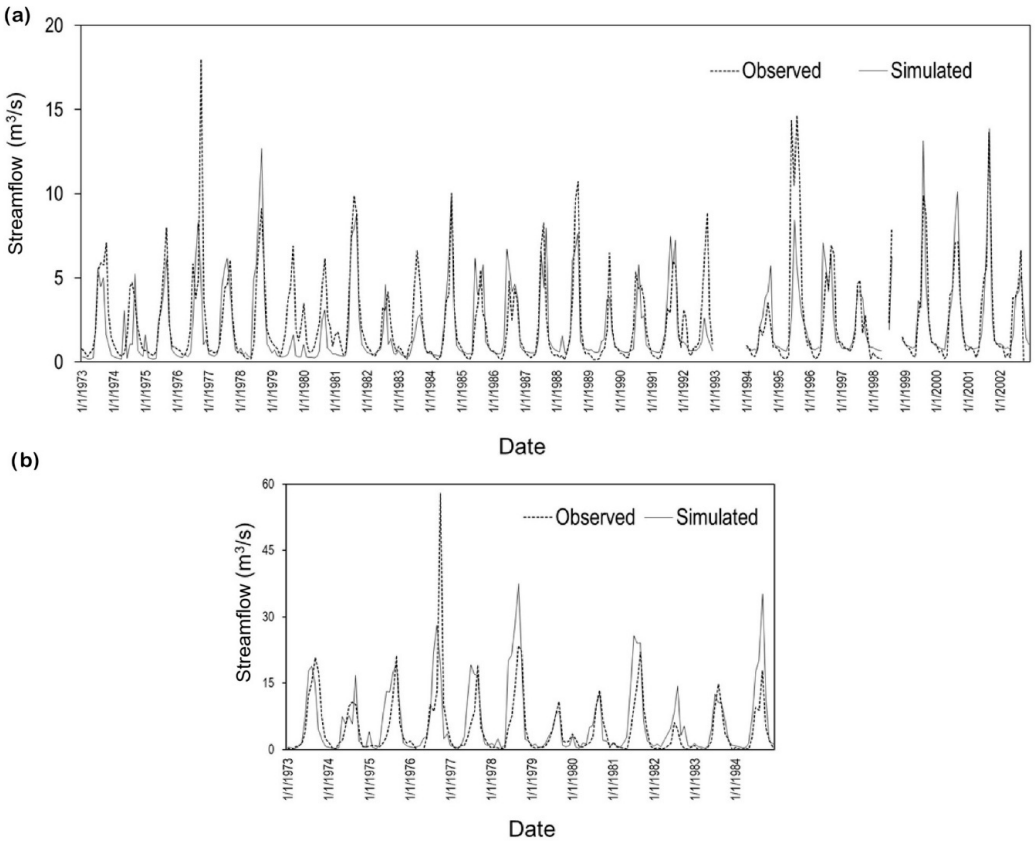



**Figure 6.** Streamflow calibration in SWAT-MODFLOW. Comparison of observed and simulated stream flow series: (**a**) HS1 from 1973–2002, and (**b**) HS2 from 1973–1984.

Groundwater model calibration was performed using data from 12 groundwater observation points (GOP) located in different geological units within the MQA, with information available for the years 2008 and 2017. Table 2 presents the observed and simulated water table levels along with the adjustments made in the GOP. Model performance was assessed using statistical adjustment metrics, MAE and RMSE, calculated for each geological unit.

The MAE varied between 4.15 and 24.03 m, while the RMSE ranged from 5.29 to 24.60 m. The best model fit was achieved in the lacustrine deposits, whereas the lowest fit was observed in the basaltic unit. In most GOP, the water table levels are underestimation. Conversely, in 2017, the model overestimated water table levels, except at the groundwater observation points located in the basalt unit. The distribution of calibrated GHCs can be found in Figure A2 in Appendix A.

**Table 2.** Comparison simulated and observed water table level by geological units and statistical metrics.

| Geological Unit | Water Table Level (2008) | | Water Table Level (2017) | | MAE [1] (m) | RMSE [1] (m) |
|---|---|---|---|---|---|---|
| | Observed (masl) | Simulated (masl) | Observed (masl) | Simulated (masl) | | |
| Volcanoclastic | 1851.85 | 1824.4 | 1803.45 | 1807.02 | 24.03 | 24.60 |
| Alluvial | 1835.45 | 1833.50 | 1825.71 | 1833.20 | 14.27 | 17.83 |
| Acid tuff | 1837.38 | 1834.62 | 1824.70 | 1833.24 | 5.66 | 6.35 |
| Lacustrine | 1836.18 | 1833.10 | 1832.03 | 1832.24 | 4.15 | 5.29 |
| Basalt | 1947.00 | 1948.67 | 1995.00 | 2013.17 | 7.33 | 10.69 |

[1] Mean a[1]Absolute error (MAE), root mean square error (RMSE).

Figure 7 illustrates both observed and simulated water table levels, with a trend showing an $R^2$ greater than 0.92. In 2008, most observation wells presented a water table level between 1857 and 1832 masl, except for those located in the basaltic rock, which exhibited levels of 2017 and 1877 masl. However, in 2017, most observation wells recorded lower water table levels, with water table levels shifting between 1788 and 1838 masl. The well located in the basaltic unit recorded a decrease of 27 m, resulting in a water table level of 1995 masl.

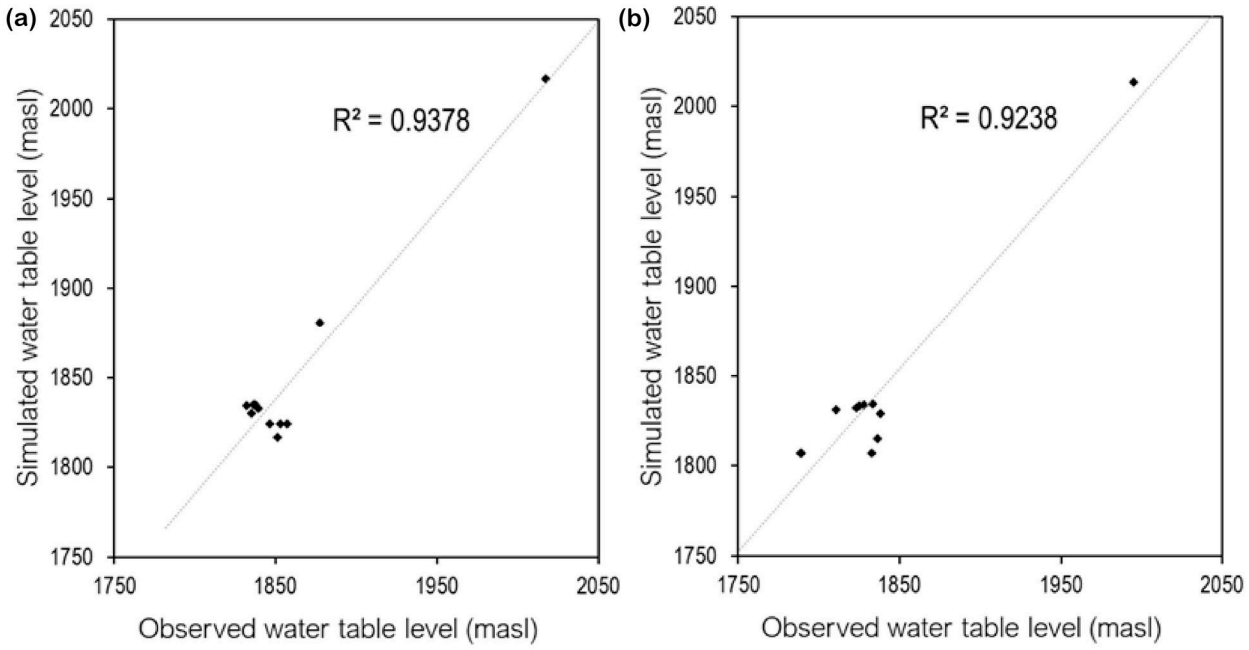



**Figure 7.** Observed and simulated water table levels for (**a**) 2008 and (**b**) 2017.

## 3. Results

### *3.1. Precipitation*

From 1973 to 2020, the mean precipitation was 854.40 mm per year, as calculated using SWAT-MODFLOW (later presented in Table 6). The M-K test was applied to the entire time

series to evaluate the presence of a monotonic trend alongside the CUSUM test, which identified five distinct periods (Table 3). The analysis revealed that the complete series from 1973 to 2020, as well as four out of the six periods analyzed (1973 to 1981, 1982 to 1990, 1991 to 1998, and 1999 to 2007), did not show a significant trend, indicating a normal variability range. However, a statistically significant dry period was observed from 2008 to 2020. The graphical analysis of the annual precipitation time series, using the CUSUM test, is shown in Figure A3a in Appendix A.

**Table 3.** Dry and wet sequences determined by the M-K test with a significance level of 0.05.

| Period | S | Z | *p*-Value | Trend | Sequence |
|---|---|---|---|---|---|
| 1973–2020 | 34 | 0.293 | 0.769 | No significant | N-S [1] |
| 1973–1981 | 8 | 0.730 | 0.466 | No significant | N-S [1] |
| 1982–1990 | 4 | 0.313 | 0.755 | No significant | N-S [1] |
| 1991–1998 | −6 | −0.620 | 0.536 | No significant | N-S [1] |
| 1999–2007 | 9 | 0.716 | 0.474 | No significant | N-S [1] |
| 2008–2020 | −40 | −2.380 | 0.017 | Significant downward | D-S [1] |

[1] Normal sequence (N-S), dry sequence (D-S).

Additionally, Student's *t*-test was applied over the same period as the M-K test, as well as over another period determined from the monthly precipitation time series (see Figure A3b in the Appendix A). This analysis indicated a significant change in mean precipitation during two couple of periods: from 1982 to 1990 compared to 1991 to 1998, and from 2008 to 2014 compared to 2015 to 2020 (Table 4). While a difference in the mean precipitation was observed between the periods 1982 to 1990 and 1991 to 1998, both the M-K test and CUSUM test suggested that the series remained within the normal variability range, with no clear evidence of a structural change.

**Table 4.** Change in mean precipitation according to Student's *t*-test for n − 2 degrees of freedom.

| Period 1 | Mean 1 | Period 2 | Mean 2 | T-Value | T-Critical ($\alpha$ = 0.05) | Significance |
|---|---|---|---|---|---|---|
| 1973–1981 | 852.69 | 1982–1990 | 785.59 | 1.41 | 1.75 | No |
| 1982–1990 | 785.59 | 1991–1998 | 901.45 | 2.3 | 1.75 | Yes |
| 1991–1998 | 901.45 | 1999–2007 | 903.19 | 0.14 | 0.14 | No |
| 1999–2007 | 903.19 | 2008–2020 | 840.90 | 1.45 | 1.72 | No |
| 2008–2014 [1] | 906.89 | 2015–2020 [1] | 762.16 | 3.25 | 1.8 | Yes |

[1] Change in the mean identified by graphical analysis (Figure A3b in Appendix A).

Figure 8 illustrates the spatial distribution of annual precipitation for the period from 1973 to 2007, which had an average annual precipitation of 863.96 mm. This period exhibited two distinct zones of precipitation: lower values, ranging from 678 to 834 mm per year, were found in the lacustrine plain, while higher values from 834 to 1252 mm per year were recorded in the highlands in the southwest of the basin.

The spatial analysis of annual precipitation trends is conducted over two periods: 1973 to 2007 and 2008 to 2020. During the first period, two trend zones are identified: an increasing trend and a non-significant trend. The non-significant trend is associated with the lowest precipitation zones of the basin, while the highest precipitation zones correspond to the increasing trend. However, during the period from 2008 to 2020, the trend shifts from increasing to decreasing, indicating a dry period (Figure 9a,b).

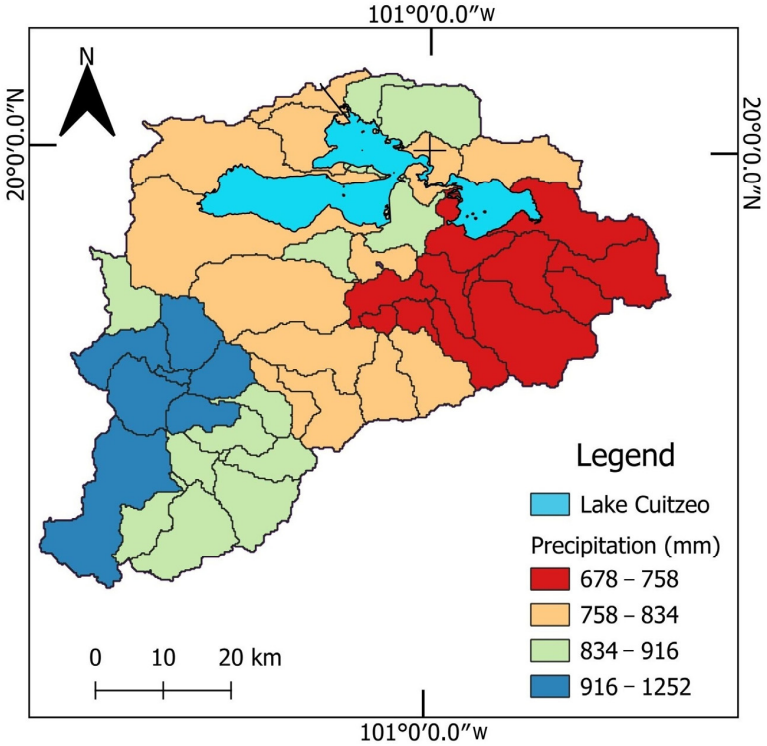



**Figure 8.** Mean annual precipitation from 1973 to 2007.

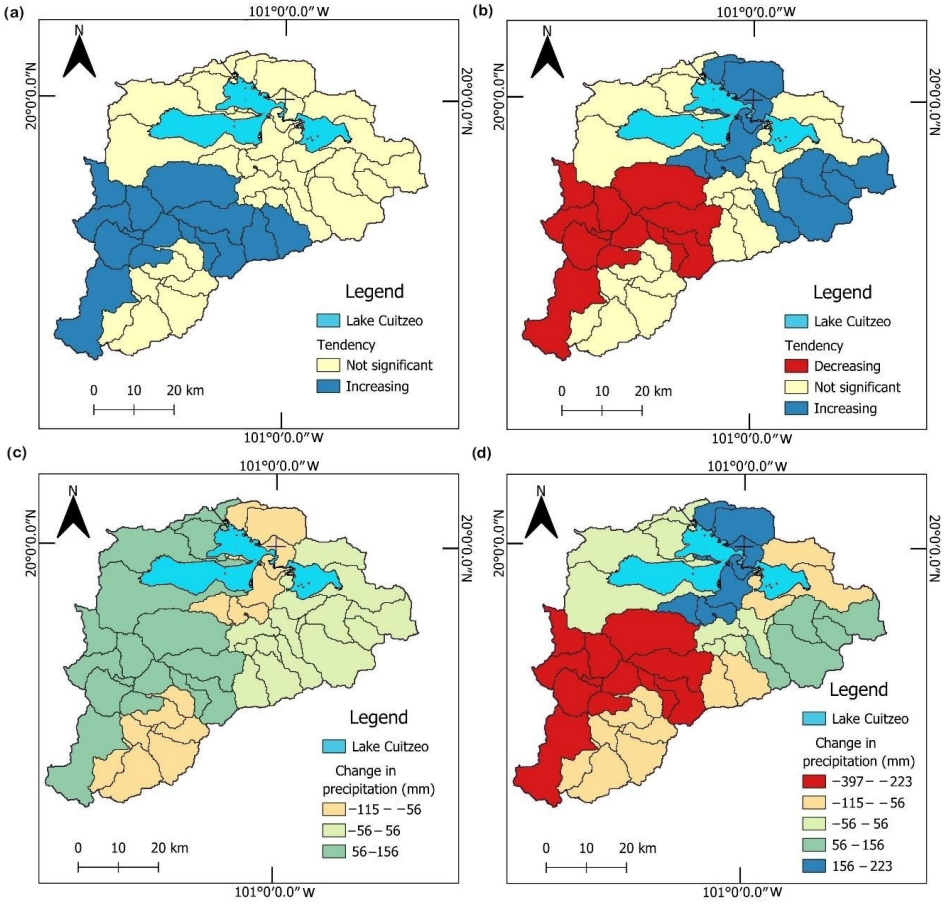



**Figure 9.** Trends analyzed by the M-K test for: (**a**) 1973 to 2007, and (**b**) 2008 to 2020. Changes in the mean annual precipitation are assessed using Student's *t*-test. Changes in mean compared to the period from 1973 to 2007 are shown for: (**c**) 2008 to 2014, and (**d**) 2015 to 2020.

Further analysis of the mean precipitation reveals an interesting change in 2015. Consequently, the spatial analysis of precipitation is divided into three periods: 1973 to 2007, 2008 to 2014, and 2015 to 2020 (Figure 9c,d). Precipitation anomalies are compared against the spatial distribution for the 1973 to 2007 period (Figure 8). In the western zone, precipitation increases by up to 155 mm per year, while in the eastern zone, it decreases by 115 mm per year. After 2008, the changes in precipitation align with the decreasing trend zone, showing lower anomalies of 397 mm per year, which represents a 46% reduction compared to the basin's average annual value of 863.96 mm. Starting in 2008, a dry period with a statistically significant downward trend emerged. In addition, within this period, a statistical change in the mean precipitation occurred beginning in 2015, showing a decrease of 10.22% compared with the mean from 1973 to 2014. Notably, this decrease is concentrated in the area with the highest precipitation within the basin.

### *3.2. Land Use and Land Cover Change*

The primary LULC (for the year 1997) in the watershed is agriculture, which accounts for approximately 39.79% and 43.09% of the aquifer area. The second most prevalent LULC is forest, encompassing deciduous, evergreen, and mixed forests, which make up about 21.56% to 23.1% of the area. Brush and range grasses are also significant, representing 20.7% to 23.95%. Other LULCs include water bodies (9%), urban areas (2.31% to 5.61%), wetlands (0.35% to 1.67%), and barren land (<1%), which make up lower percentages. Between 1997 and 2013, the most notable changes in LULC were observed in urban areas, agriculture, and evergreen forests, which each increased by 3.29% and evergreen forests by 5.76%. In contrast, mixed forests decreased by 6.69%, and grass pastures declined by 3.19%. Changes in other LULCs were generally less than 1% (Table 5).

**Table 5.** Land use and land cover distribution in LCB for 1997 and 2013.

| LULC | 1997 km$^2$ | 2013 km$^2$ | 1997% | 2013% | % Change |
|---|---|---|---|---|---|
| WETN | 65.37 | 13.76 | 1.67 | 0.35 | −1.32 |
| AGRL | 1559.13 | 1688.48 | 39.79 | 43.09 | +3.30 |
| URBN | 90.66 | 219.62 | 2.31 | 5.61 | +3.29 |
| WATR | 359.70 | 340.04 | 9.18 | 8.68 | −0.50 |
| RNGE | 481.73 | 356.73 | 12.29 | 9.10 | −3.19 |
| RNGB | 456.73 | 454.38 | 11.66 | 11.60 | −0.06 |
| FRSD | 336.59 | 312.56 | 8.59 | 7.98 | −0.61 |
| FRSE | 73.16 | 298.76 | 1.87 | 7.63 | +5.76 |
| FRST | 495.08 | 233.18 | 12.64 | 5.95 | −6.68 |
| BARR | 0.00 | 0.64 | 0.00 | 0.02 | +0.02 |

### *3.3. Changes i3.3 Change in Evapotranspiration, Surface Runoff, and Percolation*

The LULC change calculated in 2013 relative to 1997 resulted in a 26.20% increase in surface runoff. In construct, estimated evapotranspiration decreased by 1.77% (possibly induced by the decrease in forestry cover), and percolation declined by 6.34%. The hydrological balance, calculated for the 2013 LULC, applying SWAT-MODFLOW, shows only a small difference in magnitude compared to SWAT (Table 6). An uncertainty and error assessment of recharge estimates from observed and simulated surface runoff is presented in Table A2 in the Appendix A.

Figure 10 illustrates the temporal distribution of precipitation, surface runoff, evapotranspiration, and percolation. A decrease in precipitation during the period from 2015 to 2020 led to a significant 47.60% reduction in surface runoff, a 2.78% decrease in evapotranspiration, and a 36.02% decrease in percolation when using the 1997 LULC.

**Table 6.** Comparison of the effect of the land use change on the hydrological balance of the basin.

| LULC/Model | Simulated Period | Precipitation (mm) | Surface Runoff (mm) | Evapotranspiration (mm) | Percolation (mm) |
|---|---|---|---|---|---|
| LULC 1997/SWAT | 1973–2007 | 863.96 | 43.22 | 704.22 | 43.24 |
| LULC 2013/SWAT | 2008–2020 | 840.09 | 54.54 | 691.70 | 40.50 |
| LULC 2013/SWAT-MODFLOW | 1973–2020 | 854.40 | 55.36 | 693.30 | 45.32 |

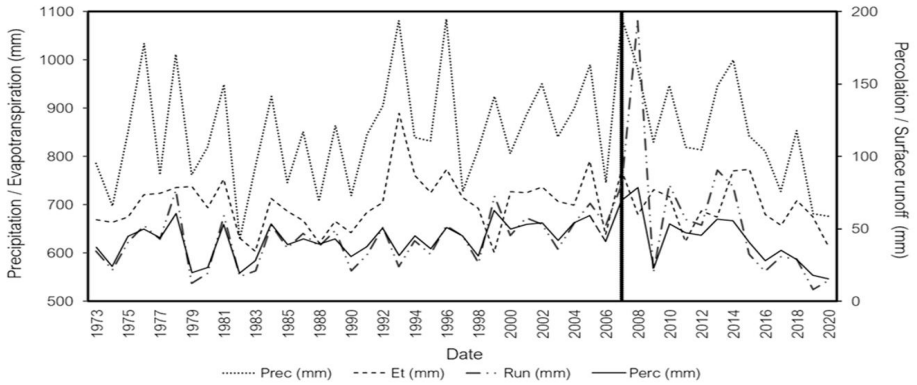



**Figure 10.** Temporal distribution of precipitation, evapotranspiration, runoff, and percolation. This figure compares LULC in 1997 for the period from 1973 to 2007, with LULC in 2013 for the period from 2008 to 2020. Precipitation (Prec), evapotranspiration (Et), surface runoff (Run), and percolation (Perc).

Evapotranspiration values range from 250 to 891 mm per year (for both LULC data), with the highest levels occurring in the southwestern part of the basin, where the combination of forest and agricultural is at its peak. Conversely, there is a decrease in these values in the central-eastern zone of the basin, largely due to the increase in urban land. In the lake plain area, evapotranspiration exhibits an increase in the eastern section and a relatively small decrease in the western section, with intervals falling between 559 and 656, and 656 and 693 mm per year (Figure 11a,b).

Surface runoff and percolation display a similar spatial pattern, closely linked to the distribution of precipitation. The highest values in the basin are found in the upper southwestern region, while the lowest values are located in the lower lakes and southeastern areas. In addition, both variables show a decrease in sub-basins experiencing dry periods, particularly in the mean values from 2015 to 2020. Notably, an increase in runoff has been observed mainly in urban areas (Figure 11c–f).

### *3.4. Groundwater Flow*

The highest percolation rates are observed in two primary areas: the southwestern zone and the northern region of the lake. However, the findings indicate that only a portion of this percolation contributes to immediate recharge. In Zone 1, it is assumed that recharge to the aquifer occurs exclusively through percolation. However, in Zone 2, located in the higher altitude area of the basin where basalts and andesites are prevalent, percolation is delayed due to the greater depth of the water table compared to the rest of the MQA. To account for this delay, the groundwater delay time coefficient is applied in the SWAT-MODFLOW model.

Figure 12a–d illustrate the water table levels at the beginning of the modeling period (after the warm-up in 1973), as well as in 1980, 1990, and after the simulation in 2020. The water table levels range from 1557 to 3080 masl, with the elevation near the lake approximately 1820 masl. In 1973, groundwater movement was primarily parallel to the basin's topography, flowing towards the lake. However, by 1980, a drawdown in the water

table was evident both in the northern and southern parts of the basin, which became more noticeable by 1990, probably due to an associated increase in agricultural and urban activities. In 2020, the water table rose to 1557.31 masl in the urban zone and 1606 masl in the northern portion of the basin. This drawdown in the water table has led to changes in the regional dynamics of groundwater flow.

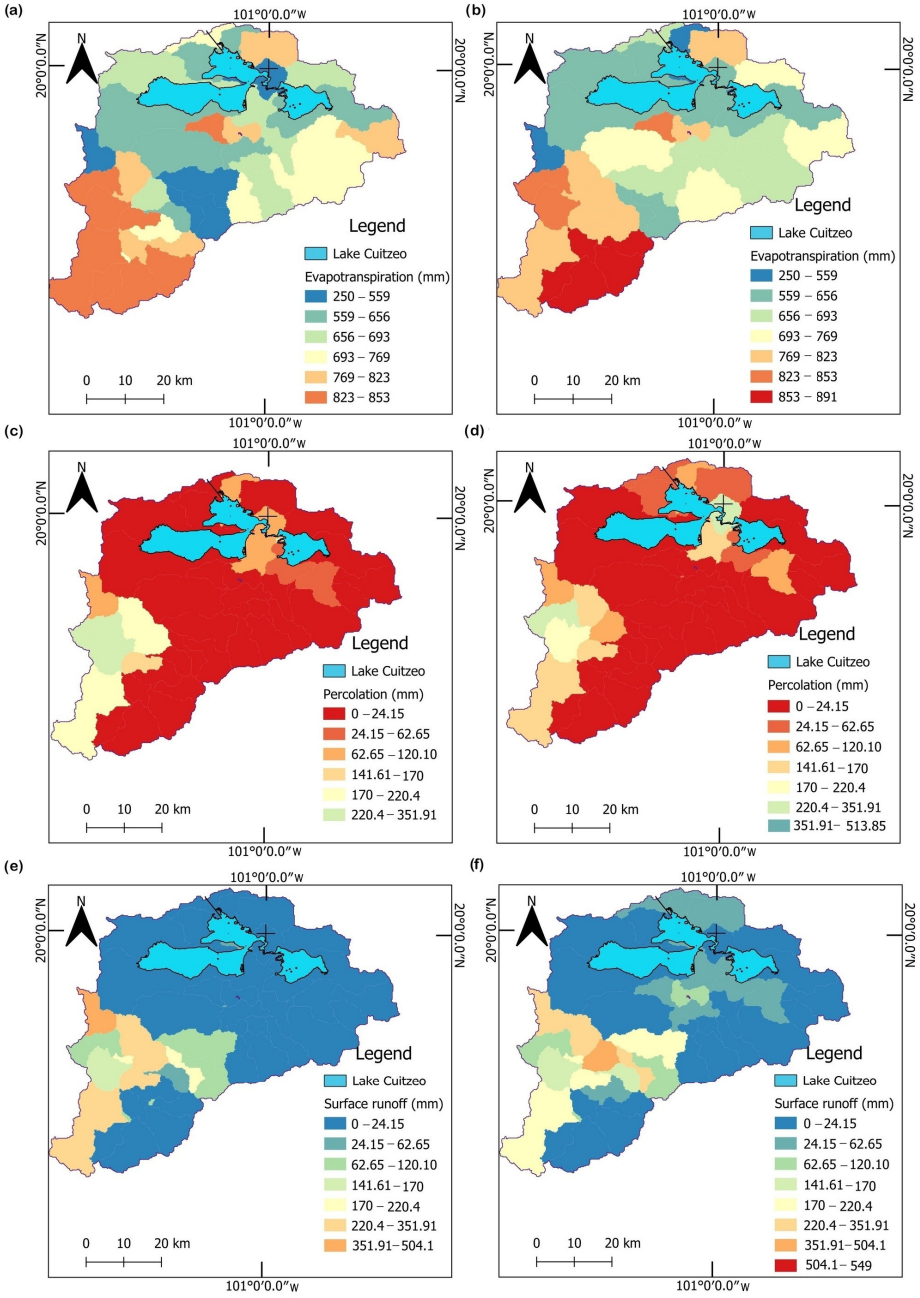



**Figure 11.** Spatial distribution of evapotranspiration (**a**,**b**), percolation (**c**,**d**), and surface runoff (**e**,**f**) for the periods 1973 to 2007 (**left**) and 2008 to 2020 (**right**). In the simulation, land use for 1997 was applied for 1973 to 2007, and land use for 2013 was applied for 2008 to 2020.

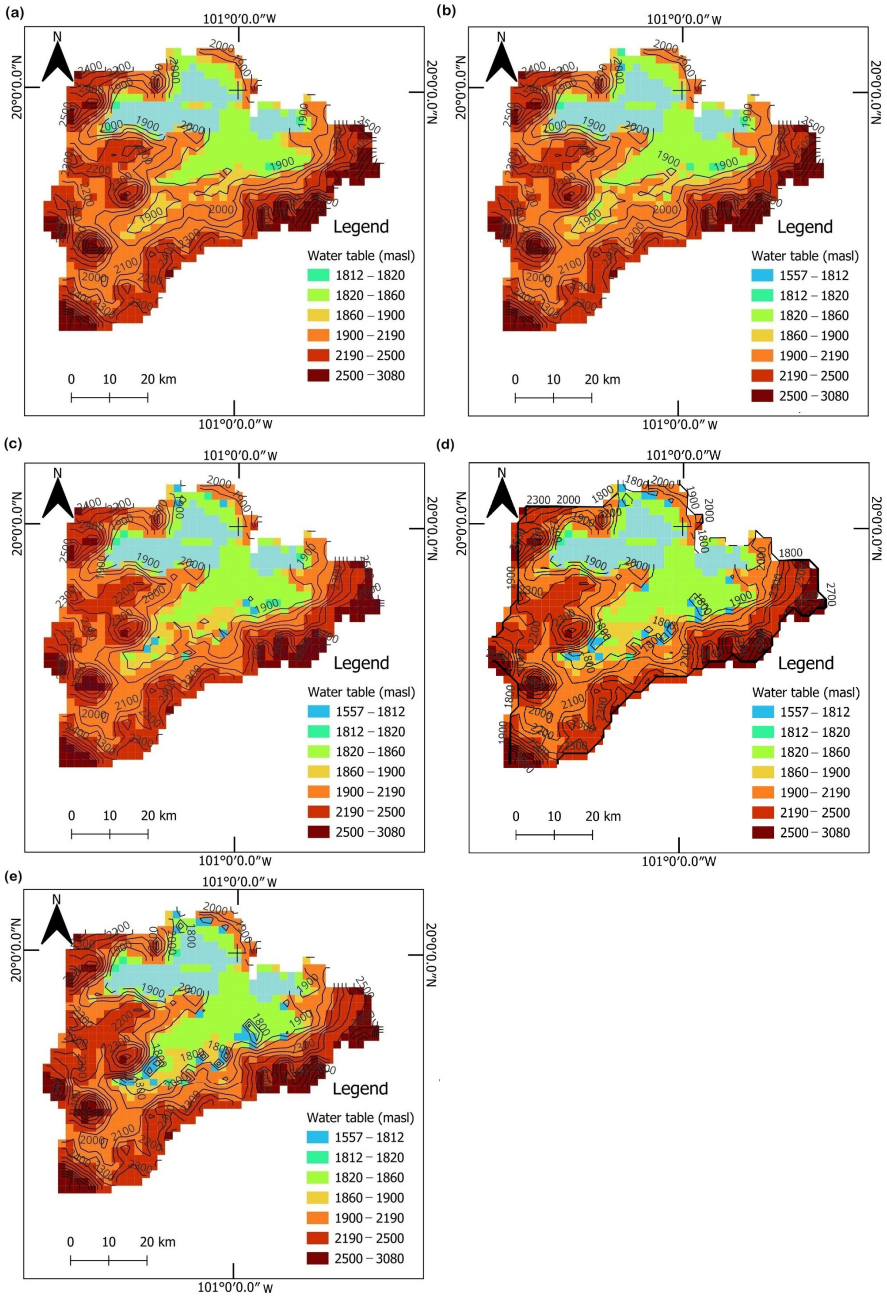



**Figure 12.** Simulated water table levels for the years (**a**) 1973, (**b**) 1980, (**c**) 1990, (**d**) 2010, and (**e**) 2020.

## 4. Discussion

This paper proposes a methodology for endorheic basins based on the spatio-temporal analysis of surface and subsurface hydrological variables to evaluate changes in hydrological patterns under climatic variability and anthropogenic pressures. The approach aims to identify the main basin-scale processes controlling lake storage dynamics, particularly under data-scarce conditions. This study provides a quantitative evaluation of the spatio-temporal pattern changes in the Lake Cuitzeo Basin through coupled SWAT-MODFLOW modeling. Mathematical modeling is an essential tool in understanding SW-GW systems. In recent years, the integration of SW-GW models has facilitated an integrated assessment of hydrological basins such as groundwater recharge and river-aquifer interactions [70,71]. The SWAT model has been widely applied globally for tasks such as calculating recharge, managing agricultural practices, and analyzing LULC changes [72–76]. Similarly, the MODFLOW model is one of the most commonly used models for GW systems analysis

worldwide [77–79]. Therefore, the coupling of SWAT and SWAT-MODFLOW enables the evaluation of various SW-GW system interactions [80,81].

The implementation of a robust mathematical model to assess various SW-GW interactions through the coupling of SWAT and SWAT-MODFLOW involves adjusting the statistical metrics used in mathematical models. Although limited data hindered a more precise calibration of the statistical metrics, the results are comparable to several studies that utilized the SWAT model [82,83] and the MODFLOW model [84,85] independently, but with the benefit of the use of an integrated and coupled hydrological model in SWAT-MODFLOW.

The relationship between the flooded area of LC and climatic variables has been established in previous studies [86]. According to this study, the precipitation time series indicates dry periods between 1940 and 1960, 1980 and 1990, and 1995 and 2000, which correspond to reductions in lake area observed in 1942, 1946, and 1962. In 1986, the LC area decreased by about 16% to 251 $km^2$, coinciding with the lowering of the water table observed since 1980, driven by reduced precipitation and increased groundwater pumping. In 2022, several media outlets reported that nearly 70% of Lake Cuitzeo had dried up as a result of extreme drought conditions [87]. Therefore, based on the aforementioned studies, a relationship can be established with the decrease in basin-scale precipitation observed since 2015. Hernández-Bedolla et al. [88] predict that climate change will lead to a 23% decrease in surface runoff and an 11.4% decrease in recharge in the southwestern region (Grande River of Morelia sub-basin) between 2015 and 2039. This decrease is attributed to a decline in mean annual precipitation ranging from 11.8% to 14.8%. In the current study, a similar decrease in precipitation of 10.22% was observed for the period from 2015 to 2020. However, due to the spatial distribution of precipitation, this corresponds to reductions of 47.60% in surface runoff and 36.02% in percolation.

The LCB is predominantly composed of agricultural soils, forests, and pastures. Changes in LULC within the LCB have been analyzed using satellite images from 1975 to 2000, with specific examinations in 1975, 1986, 1996, 2000, and 2003 [46,89]. There was a slight increase in infiltration areas during the 1975 to 2000 period, while the most significant LULC changes occurred between 1986 and 1996 (analyzed from 1975 to 2003). Following the devastating 1985 earthquake in Mexico City, substantial urban growth was recorded in Morelia, leading to a doubling of the urbanized percentage area in the basin [89].

In previous studies, the calculated mean annual values of percolation and recharge were found to be similar to those obtained in this work using the SWAT model, which showed a mean value of 161.39 $hm^3$. Other studies reported mean values of 182 $hm^3$ [90] and 169.672 $hm^3$ [91]. The difference in percolation calculated between the two land uses was 9.59 $hm^3$, with the 2013 LULC showing a higher value. These results align with Mendoza [46] who noted that areas with greater infiltration increased from 1975 to 2000. However, with the implementation of the coupled SWAT-MODFLOW model, a distinction can be made between percolation (the amount of water infiltrating from the deeper soil layer) and actual groundwater recharge (the amount of water effectively entering the aquifer). This distinction is due to the GHCs of the unalerted igneous rocks (basalt, andesite, and tuff) found in the topographically high areas of the southwest basin. The recharge zone coincides with the findings of CONAGUA [50], which calculated a mean annual percolation of 160.1 $hm^3$, based on a hydrological water balance in a portion of the aquifer near the lake (2030 $km^2$).

The GHCs of basalt are complex and understudied in the MQA. Several studies have indicated that primary porosity in basalts is not significant due to its low values, which raises concerns about the sustainability of this type of aquifer in the long term [19]. However, secondary porosity, which includes fractures and faults, plays an essential role in

the recharge and discharge of basaltic aquifers [92]. In the reviewed studies on the MQA, secondary porosity is often overlooked [50,51,69]. It is suggested that recharge in extrusive igneous rocks may involve different dynamics, such as preferential flow paths [50,69].

In the 1970s, groundwater flow was directed towards the lake plain and LC, indicating a contribution of the aquifer to the lake through the direct connection at the bottom of the lake. However, in recent years, groundwater flow has shifted from the lake towards the lake plain and the northern part of the basin. Additionally, areas with higher percolation have experienced reduced recharge due to the GHCs of igneous rock. These dynamics of groundwater flow are consistent with findings published by CONAGUA [69].

The resulting uncertainty in the estimated recharge is between 0.2495 and −1.28781 mm per year for LULC 2013 (Table A2 in Appendix A). This level of uncertainty does not affect the main conclusions regarding lake–aquifer interactions, which are primarily controlled by groundwater intensive exploitation rather than recharge variability. Simulated groundwater levels in the areas surrounding the lake fell below the lake bottom beginning in 1990 (Figure 12c), with a mean difference of about 4 m between simulated and observed levels (Table 2). These results indicate that, despite the quantified uncertainties, the direction and magnitude of lake–aquifer interactions remain robust.

The length of the streamflow record and the limited number of hydrometric stations constrain the calibration, as well as the assessment of LULC change effects. The performance at HS2 shows relatively low NSE and PBIAS values compared with those recommended in the literature [62,93]. Due to its spatial location, HS2 may reflect urban inflows or withdrawals that influence the observed streamflow; nevertheless, it provides valuable information for constraining model performance at the basin scale, and its performance is comparable to that reported in similar studies [94,95]. This overestimation may propagate into the hydrological balance components, particularly surface runoff and percolation. Furthermore, calibration under both LULC scenarios relied on the same observed stream flow data from two hydrometric stations. Consequently, the hydrological balance estimates may attenuate the apparent impact of LULC changes on percolation and groundwater recharge.

Another limitation of this study relates to the groundwater model arising from data scarcity, which requires us to discretize the aquifer as a single layer with a constant thickness of 300 m and assume constant groundwater pumping throughout the modeling period. According to CONAGUA studies, the aquifer is characterized as a single hydrogeological unit [50,69], and previous investigations of the MQA have adopted similar discretization schemes [90,91]. The assumption of constant pumping may lead to an overestimation of groundwater extraction during the early years of the simulation; however, this represents the only pumping information available for the study area. Moreover, this simplification has been applied in previous applications of MQA [90,91], and comparable assumptions are commonly reported in international groundwater modeling studies [96,97].

The representation of LC does not include a detailed model that incorporates lake characteristics, such as evaporation, water level variations, and bathymetry. The inclusion of this information would improve the representation of lake processes and could enable the identification of additional factors contributing to the observed reduction in lake storage. Incorporating lake water levels and bathymetry would allow evaporation to be estimated indirectly through water balance relationships. Previous studies have identified evaporation and lake geometry as critical controls on lake storage, especially in shallow lakes, where small decreases in water level can lead to disproportionate losses in volume [98,99]. Furthermore, representing the lake under transient conditions would allow the quantification of lake–groundwater interactions [100,101].

## 5. Conclusions

This article proposes a methodology for endorheic basins based on the spatio-temporal analysis of surface and subsurface hydrological variables to evaluate changes in hydrological patterns under climatic variability and anthropogenic pressures. The approach aims to identify the main basin-scale processes controlling lake storage dynamics, particularly under data-scarce conditions, through coupled SWAT-MODFLOW analysis of the LCB. This analysis assesses the main hydrological processes (evapotranspiration, surface runoff, percolation, groundwater recharge, and groundwater flow) and the interaction within the SW-GW system. It is particularly valuable in areas where data is limited or scarce. The analysis is carried out at the basin scale, which serves as a fundamental unit for understanding water systems.

The proposed methodology involves a mathematical model that couples basin and aquifer systems on a macro scale to evaluate their interdependent interactions. The first stage includes calibrating a SWAT model to assess precipitation at the basin scale and evaluating two different LULCs to quantify the effects of LULC changes on surface runoff, percolation, and evapotranspiration. In the second stage, the SWAT model is coupled with the MODFLOW-NWT model to evaluate recharge and groundwater flow dynamics.

Precipitation and LULC changes at the basin scale are treated as independent variables in SWAT, while the dependent variables include surface runoff, evapotranspiration, percolation, recharge, and groundwater flow. Precipitation is analyzed using comprehensive graphical and statistical analysis to identify statistically significant trends and changes in order to identify points of change, trends, and quantify whether a statistically significant change is occurring. For its part, land use is quantified in terms of its relative change since 1997 and is used as input information to assess its effect on the main hydrological processes within the hydrological model.

Once the effect of precipitation and LULC change has been analyzed, the SWAT-MODFLOW model is coupled to quantify recharge. The implementation of a coupled model facilitates the creation of a robust coupled model, which helps reduce uncertainties associated with mathematical modeling while providing significant temporal and spatial discretization of variables affecting lake storage. Despite the limited information available from the study area, the calibration achieved with the SWAT model and SWAT-MODFLOW is deemed acceptable. Furthermore, the statistical metrics for two LULCs in the surface runoff and percolation analysis indicate that the SWAT model effectively predicts SW processes.

The results show that due to climate change and anthropogenic activities, changes in regional hydrological dynamics have substantially altered groundwater flow within the basin. The decreases in precipitation have reduced percolation rates and, when combined with groundwater extraction and GHCs of the aquifer, have led to a notable drop in water table levels, thereby altering groundwater flow dynamics. The evidence of the impact of anthropogenic activities within the basin indicates that the lake once consistently received water from the aquifer. However, due to the effect of climate change on hydrological processes, GHCs, and groundwater extraction, the regional groundwater flow has been altered, causing the lake to contribute to groundwater flow and leading to a substantial reduction in its storage.

This study shows the complexity of hydrological processes in endorheic basins and their SW-GW interactions. The results show the effect of climatic variables, such as precipitation, and the influence of anthropogenic activities, such as withdrawals and land use change. The combination of climate change and human pressure has reversed the flow between the lake and the aquifer, causing a significant decrease in lake water levels. These findings underscore the vulnerability of endorheic basins to natural and anthro-

pogenic changes and highlight the need to develop more detailed simulation models that incorporate surface–subsurface interactions.

This study is presented as the first to evaluate the interactions between the surface and underground systems in order to understand their effect on the storage capacity of LC. Although this initial model has several limitations due to data scarcity, the main constraints include the lack of a detailed representation of the lake and the limited length of the streamflow series. In addition, the model excludes other groundwater processes, such as preferential groundwater flows and spring discharges. These limitations could result in an underestimation in the calculation of percolation and recharge. Nevertheless, the groundwater flow model was calibrated with acceptable results, providing a useful basis for evaluating lake–aquifer interactions.

Future research should address the limitations of this study by employing a more complex simulation setup, including the detailed integration of the lake and other processes into the groundwater flow model. This will enable the conceptual representation of the lake and the quantification of its water balance at the basin scale. Additionally, future studies should evaluate the short- and long-term effects of climate change by incorporating precipitation and temperature to assess their impact on groundwater recharge and lake storage, and also evaluate measures for the recovery of the LC.

**Author Contributions:** Conceptualization, J.H.-B. and A.C.-G.; methodology, A.C.-G. and M.A.H.-H.; software, M.A.M.-C. and J.H.-B.; validation, S.T.S.-Q., A.C.-G. and J.H.-B.; formal analysis, M.A.H.-H. and A.C.-G.; investigation, J.H.-B. and S.T.S.-Q.; resources, M.A.H.-H. and C.D.S.; data curation, M.A.H.-H.; writing—original draft preparation, S.T.S.-Q. and A.C.-G.; writing—review and editing, M.A.H.-H. and S.T.S.-Q.; visualization, M.A.M.-C.; supervision, S.T.S.-Q.; project administration, M.A.H.-H.; funding acquisition, C.D.S., M.A.M.-C. and S.T.S.-Q. All authors have read and agreed to the published version of the manuscript.

**Funding:** This work was supported by "Programa de apoyo a proyectos de investigación e innovación tecnológica", UNAM-PAPIIT 2023, TA101123, and SECIHTI-IxM Program, Project P58.

**Data Availability Statement:** The original contributions presented in this study are included in the article. Further inquiries can be directed to the corresponding author.

**Acknowledgments:** The authors would like to thank the Graduate Program in Chemical Engineering and the Hydraulics Department at the Universidad Michoacana de San Nicolás de Hidalgo for their support. They also extend their gratitude to the Secretariat of Science, Technology, and Innovation of Mexico City (SECIHTI) for the scholarship granted to one of the authors.

**Conflicts of Interest:** The authors declare no conflicts of interest.

## Abbreviations

The following abbreviations are used in this manuscript:

| | |
|---|---|
| CUSUM | Cumulative sum |
| DEM | Digital elevation model |
| LCB | Lake Cuitzeo Basin |
| LC | Lake Cuitzeo |
| LULC | Land use and land cover |
| HRU | Hydrological Response Units |
| HS | Hydrometric stations |
| GHCs | Geohydrological characteristics |
| GOP | Groundwater observation points |
| MQA | Morelia-Queréndaro aquifer |
| M-K | Mann–Kendall |
| SW-GW | Surface water and groundwater |

# Appendix A

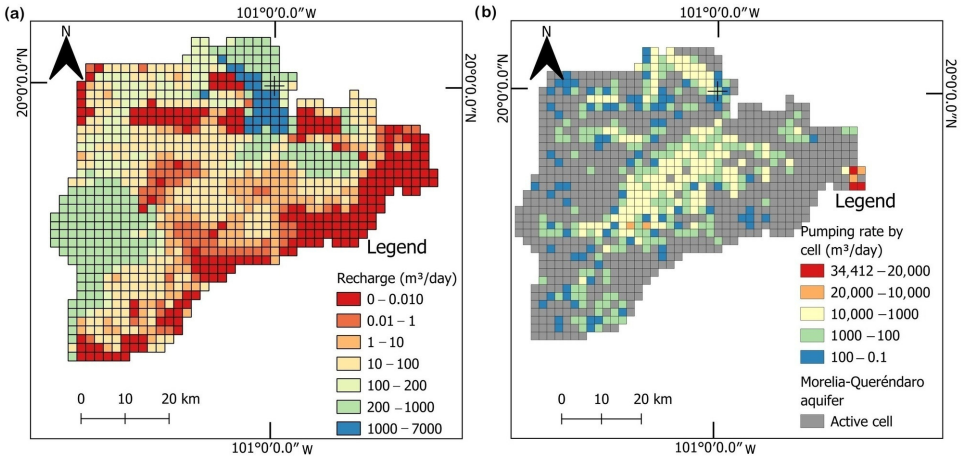



**Figure A1.** Model configuration in SWAT-MODFLOW for the modeling period of 1973–2020. (**a**) Recharge discretization calculated in SWAT with annual mean values, and (**b**) Pumping rate distribution (in $m^3$ per day) with constant values throughout the modeling period.

**Table A1.** Model Parameter Ranges and Calibration Values by Land Use and Land Cover.

| Parameter | Range | Units | AGRL | FRSD | FRSE | FRST | RNGE | RNGB | WATR | BARR | WETN | URBN |
|---|---|---|---|---|---|---|---|---|---|---|---|---|
| ESCO | 0–1 | dimensionless | 0.7 | 0.7 | 0.675 | 0.7 | 0.6 | 0.6 | 0.01 | 0.65 | 0.5 | 0.01 |
| EPCO | 0–1 | dimensionless | 0.65 | 0.675 | 0.675 | 0.675 | 0.625 | 0.625 | 0.01 | 0.7 | 0.6 | 0.01 |
| LAT_TIME | 0–180 | days | 40 | 40 | 40 | 40 | 40 | 40 | 40 | 40 | 40 | 40 |
| SURLAG | 0–24 | days | 10 | 10 | 10 | 10 | 10 | 10 | 10 | 10 | 10 | 10 |
| ALPHA_BF | 0–1 | days | 0.08 | 0.08 | 0.08 | 0.08 | 0.08 | 0.08 | 0.08 | 0.08 | 0.08 | 0.08 |

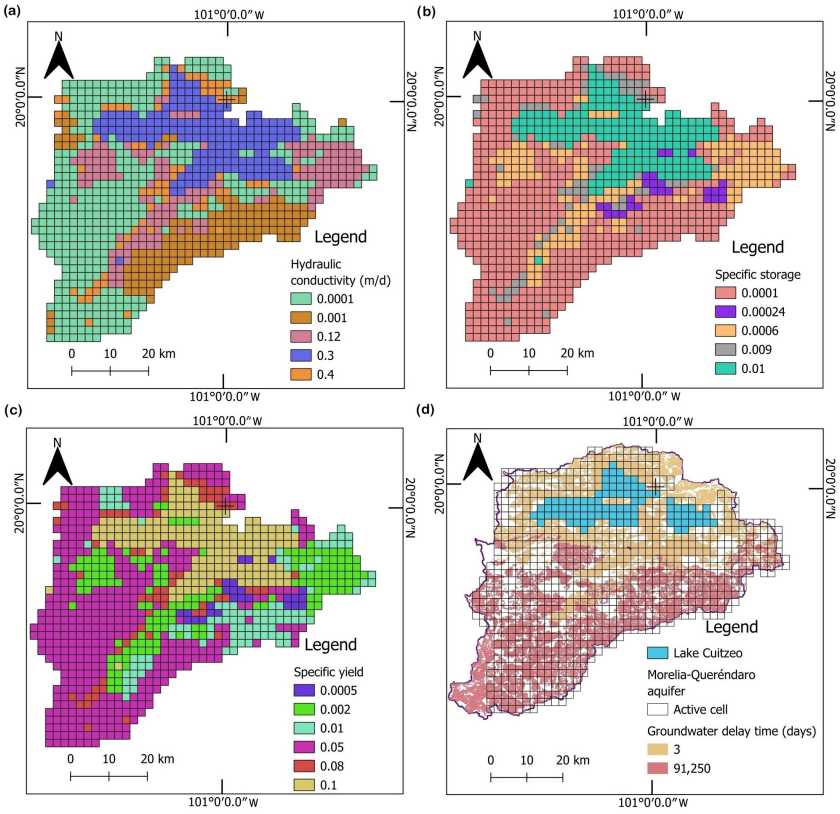



**Figure A2.** Spatial distribution of calibrated values. (**a**) Hydraulic conductivity, in m per day; (**b**) specific storage (adim); (**c**) specific yield (adim); and (**d**) groundwater delay time, in days.

**Table A2.** Uncertainty and error assessment of recharge estimates from observed and simulated surface runoff.

| LULC/Model | Station | Period | Streamflow | | | Recharge | |
|---|---|---|---|---|---|---|---|
| | | | O.M. [1] $m^3/s$ | S.M. [1] $m^3/s$ | Error $m^3/s$ | Error m | Error mm/año |
| LULC 1997/SWAT Calibration | HS1 | 1973–2002 | 2.36 | 2.01 | 0.35 | 0.0028 | 0.2817 |
| | HS2 | 1973–1984 | 4.6 | 4.96 | −0.36 | −0.0029 | −0.2898 |
| LULC 2013/SWAT Validation | HS1 | 1973–2002 | 2.36 | 2.11 | 0.25 | 0.0020 | 0.2012 |
| | HS2 | 1973–1984 | 4.6 | 5.02 | −0.42 | −0.0034 | −0.3381 |
| LULC 2013/SWAT-MODFLOW | HS1 | 1973–2002 | 2.36 | 2.05 | 0.31 | 0.0025 | 0.2495 |
| | HS2 | 1973–1984 | 4.6 | 6.2 | −1.6 | −0.0129 | −1.2878 |

[1] Observed monthly mean (O.M.), simulated monthly mean (S.M.).

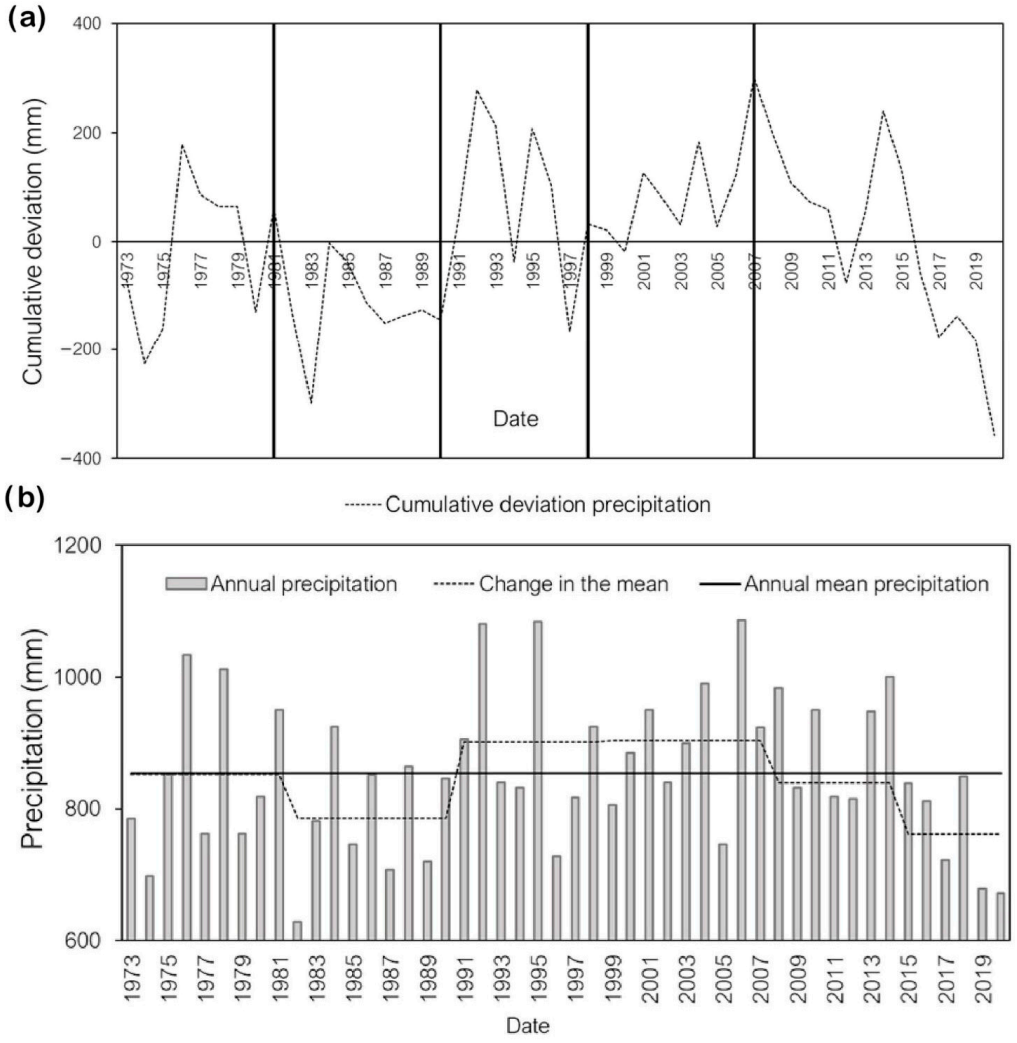



**Figure A3.** Graphical analysis: (**a**) dry and wet sequences, and (**b**) changes in mean precipitation according to Student's *t*-test for n − 2 degrees of freedom.

## References

1. Ahmad, W.; Iqbal, J.; Nasir, M.J.; Ahmad, B.; Khan, M.T.; Khan, S.N.; Adnan, S. Impact of Land Use/Land Cover Changes on Water Quality and Human Health in District Peshawar Pakistan. *Sci. Rep.* **2021**, *11*, 16526. [CrossRef]
2. Mishra, R.K. Fresh Water Availability and Its Global Challenge. *Br. J. Multidiscip. Adv. Stud.* **2023**, *4*, 1–78. [CrossRef]

3. Van, V.; Michelle, T.H.; Thorslund, J.; Strokal, M.; Hofstra, N.; Flörke, M.; Ehalt Macedo, H.; Nkwasa, A.; Tang, T.; Kaushal, S.S.; et al. Global River Water Quality under Climate Change and Hydroclimatic Extremes. *Nat. Rev. Earth Environ.* **2023**, *4*, 687–702. [CrossRef]
4. Boitt, M.K.; Albright, O.M.; Kipkulei, H.K. Assessment of Soil Erosion and Climate Variability on Kerio Valley Basin, Kenya. *J. Geosci. Environ. Prot.* **2020**, *8*, 97–114. [CrossRef]
5. Fuentealba, M.; Bahamóndez, C.; Sarricolea, P.; Meseguer-Ruiz, O.; Latorre, C. The 2010–2020 "megadrought" Drives Reduction in Lake Surface Area in the Andes of Central Chile (32o-36oS). *J. Hydrol. Reg. Stud.* **2021**, *38*, 100952. [CrossRef]
6. Kalsido, T.; Berhanu, B. Impact of Land-Use Changes on Sediment Load and Capacity Reduction of Lake Ziway, Ethiopia. *Nat. Resour.* **2020**, *11*, 530–542. [CrossRef]
7. Sophocleous, M. Interactions between Groundwater and Surface Water: The State of the Science. *Hydrogeol. J.* **2002**, *10*, 52–67. [CrossRef]
8. Mei, C.; Liu, J.; Huang, Z.; Wang, H.; Wang, K.; Shao, W.; Li, M. Spatiotemporal Pattern Variations of Daily Precipitation Concentration and Their Relationship with Possible Causes in the Yangtze River Delta, China. *J. Water Clim. Change* **2022**, *13*, 1583–1598. [CrossRef]
9. Sun, Q.; Zhang, X.; Zwiers, F.; Westra, S.; Alexander, L.V. A Global, Continental, and Regional Analysis of Changes in Extreme Precipitation. *J. Clim.* **2021**, *34*, 243–258. [CrossRef]
10. Zeng, X.; Hu, Z.; Chen, A.; Yuan, W.; Hou, G.; Han, D.; Liang, M.; Di, K.; Cao, R.; Luo, D. The Global Decline in the Sensitivity of Vegetation Productivity to Precipitation from 2001 to 2018. *Glob. Change Biol.* **2022**, *28*, 6823–6833. [CrossRef]
11. Daramola, M.T.; Xu, M. Recent Changes in Global Dryland Temperature and Precipitation. *Int. J. Climatol.* **2022**, *42*, 1267–1282. [CrossRef]
12. Thoithi, W.; Blamey, R.C.; Reason, C.J.C. Dry Spells, Wet Days, and Their Trends Across Southern Africa During the Summer Rainy Season. *Geophys. Res. Lett.* **2021**, *48*, e2020GL091041. [CrossRef]
13. Xiong, J.; Guo, S.; Chen, J.; Yin, J. Global Evaluation of the "Dry Gets Drier, and Wet Gets Wetter" Paradigm from a Terrestrial Water Storage Change Perspective. *Hydrol. Earth Syst. Sci.* **2022**, *26*, 6457–6476. [CrossRef]
14. Onyutha, C. Graphical-Statistical Method to Explore Variability of Hydrological Time Series. *Hydrol. Res.* **2021**, *52*, 266–283. [CrossRef]
15. Sam, M.G.; Nwaogazie, I.L.; Ikebude, C. Establishing Climatic Change on Rainfall Trend, Variation and Change Point Pattern in Benin City, Nigeria. *Int. J. Environ. Clim. Change* **2023**, *13*, 202–212. [CrossRef]
16. Schreiner-McGraw, A.P.; Ajami, H. Combined Impacts of Uncertainty in Precipitation and Air Temperature on Simulated Mountain System Recharge from an Integrated Hydrologic Model. *Hydrol. Earth Syst. Sci.* **2022**, *26*, 1145–1164. [CrossRef]
17. Reinecke, R.; Müller Schmied, H.; Trautmann, T.; Andersen, L.S.; Burek, P.; Flörke, M.; Gosling, S.N.; Grillakis, M.; Hanasaki, N.; Koutroulis, A.; et al. Uncertainty of Simulated Groundwater Recharge at Different Global Warming Levels: A Global-Scale Multi-Model Ensemble Study. *Hydrol. Earth Syst. Sci.* **2021**, *25*, 787–810. [CrossRef]
18. Hocking, M.; Kelly, B.F.J. Groundwater Recharge and Time Lag Measurement through Vertosols Using Impulse Response Functions. *J. Hydrol.* **2016**, *535*, 22–35. [CrossRef]
19. Du, Q.; Ross, M. Timescale of Groundwater Recharge in High Percolation Coastal Plain Soils. *Water* **2024**, *16*, 1320. [CrossRef]
20. Ali, S.; Li, D.; Congbin, F.; Khan, F. Twenty First Century Climatic and Hydrological Changes over Upper Indus Basin of Himalayan Region of Pakistan. *Environ. Res. Lett.* **2015**, *10*, 014007. [CrossRef]
21. Kite, G.W. Application of a Land Class Hydrological Model to Climatic Change. *Water Resour. Res.* **1993**, *29*, 2377–2384. [CrossRef]
22. Karlsson, I.B.; Sonnenborg, T.O.; Refsgaard, J.C.; Trolle, D.; Børgesen, C.D.; Olesen, J.E.; Jeppesen, E.; Jensen, K.H. Combined Effects of Climate Models, Hydrological Model Structures and Land Use Scenarios on Hydrological Impacts of Climate Change. *J. Hydrol.* **2016**, *535*, 301–317. [CrossRef]
23. Sun, J.; Xiao, J.; Li, Z.; Lai, G.; Du, J.; Xie, S.; Xu, X.; Meng, L.; Li, X.; Zhong, K. Effect of Calculation Unit Division in Distributed Hydrological Models on the Analysis of Hydrological Effects of Land Use Change. *Catena* **2024**, *246*, 108445. [CrossRef]
24. Tezel, A.Ç.; Akpınar, A.; Bor, A.; Alfredsen, K.T. Exploring Hydrological Response to Land Use/Land Cover Change Using the SWAT+ Model in the İznik Lake Watershed, Türkiye. *Water* **2025**, *17*, 1924. [CrossRef]
25. Scanlon, B.R.; Healy, R.W.; Cook, P.G. Choosing Appropriate Techniques for Quantifying Groundwater Recharge. *Hydrogeol. J.* **2002**, *10*, 18–39. [CrossRef]
26. Jyrkama, M.I.; Sykes, J.F.; Normani, S.D. Recharge Estimation for Transient Ground Water Modeling. *Groundwater* **2002**, *40*, 638–648. [CrossRef] [PubMed]
27. Kalogiannidis, S.; Kalfas, D.; Giannarakis, G.; Paschalidou, M. Integration of Water Resources Management Strategies in Land Use Planning towards Environmental Conservation. *Sustainability* **2023**, *15*, 15242. [CrossRef]
28. Narendra, B.H.; Siregar, C.A.; Dharmawan, I.W.S.; Sukmana, A.; Pratiwi; Pramono, I.B.; Basuki, T.M.; Nugroho, H.Y.S.H.; Supangat, A.B.; Purwanto; et al. A Review on Sustainability of Watershed Management in Indonesia. *Sustainability* **2021**, *13*, 11125. [CrossRef]

29. Furman, A. Modeling Coupled Surface–Subsurface Flow Processes: A Review. *Vadose Zone J.* **2008**, *7*, 741–756. [CrossRef]
30. Garcia-Castellanos, D.; Vergés, J.; Gaspar-Escribano, J.; Cloetingh, S. Interplay between Tectonics, Climate, and Fluvial Transport during the Cenozoic Evolution of the Ebro Basin (NE Iberia). *J. Geophys. Res. Solid Earth* **2003**, *108*, 2347. [CrossRef]
31. Aranda-Gómez, J.J.; Carranza-Castañeda, O.; Wang, X.; Tseng, Z.J.; Pacheco-Castro, A. Notes on the Origin of Extensive Endorheic Regions in Central and Northern Mexico, and Some Implications for Paleozoogeography. *J. S. Am. Earth Sci.* **2018**, *83*, 55–67. [CrossRef]
32. Marenssi, S.A.; Limarino, C.O.; Schencman, L.J.; Ciccioli, P.L. Tectonic and Geomorphic Controls on the Lacustrine Deposits of the Neogene Vinchina Basin, Northwestern Argentina. *J. Sediment. Res.* **2020**, *90*, 250–267. [CrossRef]
33. El-Azhari, A.; Ait Brahim, Y.; Barbecot, F.; Hssaisoune, M.; Berrouch, H.; Laamrani, A.; Hadri, A.; Brouziyne, Y.; Bouchaou, L. Evaluating Groundwater Salinity Patterns and Spatiotemporal Dynamics in Complex Endorheic Aquifer Systems. *Sci. Total Environ.* **2025**, *994*, 180055. [CrossRef]
34. Wei, X.; Bailey, R.T. Evaluating Nitrate and Phosphorus Remediation in Intensively Irrigated Stream-Aquifer Systems Using a Coupled Flow and Reactive Transport Model. *J. Hydrol.* **2021**, *598*, 126304. [CrossRef]
35. Park, S.; Nielsen, A.; Bailey, R.T.; Trolle, D.; Bieger, K. A QGIS-Based Graphical User Interface for Application and Evaluation of SWAT-MODFLOW Models. *Environ. Model. Softw.* **2019**, *111*, 493–497. [CrossRef]
36. Banerjee, D.; Ganguly, S. A Review on the Research Advances in Groundwater–Surface Water Interaction with an Overview of the Phenomenon. *Water* **2023**, *15*, 1552. [CrossRef]
37. Preetha, P.P.; Joseph, N.; Narasimhan, B. Quantifying Surface Water and Ground Water Interactions Using a Coupled SWAT_FEM Model: Implications of Management Practices on Hydrological Processes in Irrigated River Basins. *Water Resour. Manag.* **2021**, *35*, 2781–2797. [CrossRef]
38. Wang, Y.; Chen, N. Recent Progress in Coupled Surface–Ground Water Models and Their Potential in Watershed Hydro-Biogeochemical Studies: A Review. *Watershed Ecol. Environ.* **2021**, *3*, 17–29. [CrossRef]
39. Bailey, R.T.; Wible, T.C.; Arabi, M.; Records, R.M.; Ditty, J. Assessing Regional-Scale Spatio-Temporal Patterns of Groundwater–Surface Water Interactions Using a Coupled SWAT-MODFLOW Model. *Hydrol. Process* **2016**, *30*, 4420–4433. [CrossRef]
40. Arnold, J.G.; Moriasi, D.N.; Gassman, P.W.; Abbaspour, K.C.; White, M.J.; Srinivasan, R.; Santhi, C.; Harmel, R.D.; Van Griensven, A.; Van Liew, M.W.; et al. SWAT: Model Use, Calibration, and Validation. *Trans. ASABE* **2012**, *55*, 1491–1508. [CrossRef]
41. Li, Z.; Xue, W.; Sereewatthanawut, I. Evaluation of Best Management Practices (BMPs) for Mitigating Non-Point Source Pollution in the Wang River Basin of Thailand Based on the SWAT Model. *Environ. Technol. Innov.* **2025**, *39*, 104327. [CrossRef]
42. Fang, X.; He, W.; Wen, F.; An, M.; Wang, B.; Cheng, B. SWAT Model Application for Calculating Ecological Flow in Sub-Basins of the Huangshui River Basin. *J. Environ. Manag.* **2025**, *380*, 124837. [CrossRef] [PubMed]
43. Liu, R.; Liu, Y.; Jiao, L.; Wang, L. Multi-Objective Optimization of Reservoir Group Operation after Inter-basin Water Transfer Jointing SWAT Model and NSGA-II. *J. Hydrol.* **2025**, *660*, 133431. [CrossRef]
44. Richard, G.; Niswonger, S.P.M.I. MODFLOW-NWT, a Newton Formulation for MODFLOW-2005. *US Geol. Surv. Tech. Methods* **2011**, *6*, 44.
45. McDonald, M.; Harbaugh, A.W. A Modular Three-Dimensional Finite Difference Ground-Water Flow Model. In *Techniques of Water-Resources Investigations Book 6*; US Geological Survey: Reston, VA, USA, 1988; p. 588.
46. Mendoza, M.E.; Bocco, G.; López-Granados, E.; Bravo Espinoza, M. Hydrological Implications of Land Use and Land Cover Change: Spatial Analytical Approach at Regional Scale in the Closed Basin of the Cuitzeo Lake, Michoacan, Mexico. *Singap. J. Trop. Geogr.* **2010**, *31*, 197–214. [CrossRef]
47. Forbes Staff. *Forbes*; Forbes Staff: Jersey, NJ, USA, 2021.
48. Granados, E.L.; Mendoza, M.; Acosta, A. Cambio de Cobertura Vegetal y Uso de La Tierra. El Caso de La Cuenca Endorreica Del Lago de Cuitzeo, Michoacán. *Gac. Ecológica* **2002**, *64*, 19–34.
49. Mendoza, M.E.; Boceo, G.; Granados, E.L.; Bravo, M. Tendencias Recientes de Las Superficies Ocupadas Por El Lago de Cuitzeo. Un Enfoque Basado En Percepción Remota, Sistemas de Información Geográfica y Análisis Estadístico. *Investig. Geogr.* **2007**, *64*, 43–62.
50. CONAGUA. *Actualización de la Disponibilidad Media Anual de Agua En El Acuífero Morelia-Queréndaro (1602), Estado de Michoacán*; CONAGUA: Mexico City, Mexico, 2024. Available online: https://www.gob.mx/conagua (accessed on 3 December 2025).
51. CONAGUA. *Actualización de la Disponibilidad Media Anual de Agua En El Acuífero Morelia-Queréndaro (1602), Estado de Michoacán*; CONAGUA: Mexico City, Mexico, 2009. Available online: https://www.gob.mx/conagua (accessed on 3 December 2025).
52. Winston, R. ModelMuse—A Graphical User Interface for MODFLOW–2005 and PHAST. In *U.S. Geological Survey Techniques and Methods*; US Geological Survey: Reston, VA, USA, 2009; Volume 6.
53. Neitsch, S.L.; Arnold, J.G.; Kiniry, J.R.; Williams, J.R. *College of Agriculture and Life Sciences Soil and Water Assessment Tool. Theoretical Documentation Version 2009*; Texas Water Resources Institute: College Station, TX, USA, 2011. Available online: https://swat.tamu.edu/media/99192/swat2009-theory.pdf (accessed on 3 December 2025).

54. Mubialiwo, A.; Abebe, A.; Onyutha, C. Changes in Extreme Precipitation over Mpologoma Catchment in Uganda, East Africa. *Heliyon* **2023**, *9*, e14016. [CrossRef] [PubMed]
55. Pettitt, A.N. A Non-Parametric Approach to the Change-Point Problem. *Appl. Stat.* **1979**, *28*, 126. [CrossRef]
56. Gaddikeri, V.; Sarangi, A.; Singh, D.K.; Jatav, M.S.; Rajput, J.; Kushwaha, N.L. Trend and Change-Point Analyses of Meteorological Variables Using Mann–Kendall Family Tests and Innovative Trend Assessment Techniques in *New Bhupania* Command (India). *J. Water Clim. Change* **2024**, *15*, 2033–2058. [CrossRef]
57. Samy, A.; G. Ibrahim, M.; Mahmod, W.E.; Fujii, M.; Eltawil, A.; Daoud, W. Statistical Assessment of Rainfall Characteristics in Upper Blue Nile Basin over the Period from 1953 to 2014. *Water* **2019**, *11*, 468. [CrossRef]
58. Sridhar, S.I.; Raviraj, A. Statistical Trend Analysis of Rainfall in Amaravathi River Basin Using Mann-Kendall Test. *Curr. World Environ.* **2017**, *12*, 89–96. [CrossRef]
59. Ghebreyesus, D.; Sharif, H.O. Time Series Analysis of Monthly and Annual Precipitation in The State of Texas Using High-Resolution Radar Products. *Water* **2021**, *13*, 982. [CrossRef]
60. Lim Kam Sian, K.T.C.; Wang, J.; Ayugi, B.O.; Nooni, I.K.; Ongoma, V. Multi-Decadal Variability and Future Changes in Precipitation over Southern Africa. *Atmosphere* **2021**, *12*, 742. [CrossRef]
61. Miller, W.P.; Piechota, T.C. Regional Analysis of Trend and Step Changes Observed in Hydroclimatic Variables around the Colorado River Basin. *J. Hydrometeorol.* **2008**, *9*, 1020–1034. [CrossRef]
62. Moriasi, D.N.; Arnold, J.G.; Van Liew, M.W.; Bingner, R.L.; Harmel, R.D.; Veith, T.L. *Model Evaluation Guidelines for Systematic Quantification of Accuracy in Watershed Simulations*; American Society of Agricultural and Biological Engineers: St. Joseph, MI, USA, 2007; Volume 50.
63. CONAGUA. *Banco Nacional de Datos de Aguas Superficiales (BANDAS)*; CONAGUA: Mexico City, Mexico, 2008. Available online: https://www.imta.gob.mx/media/iframes/bandas.html (accessed on 3 December 2025).
64. Serratos, L.; Douglas, A. *NAME: Mexico Climatological Station Network Data (CLICOM); Version 1.0*; UCAR/NCAR–Earth Observing Laboratory: Boulder, CO, USA, 2007.
65. CONAGUA. Servicio Meteorológico Nacional (SMN). Available online: https://smn.conagua.gob.mx/es/climatologia/informacion-climatologica/informacion-estadistica-climatologica (accessed on 14 July 2025).
66. INEGI. *Usa La Estadística y La Geografía Para Descubrir México*; INEGI: Aguascalientes, Mexico, 2025. Available online: https://cuentame.inegi.org.mx/descubre/ (accessed on 3 December 2025).
67. Hargreaves, G.H.; Samani, Z.A. Samani Reference Crop Evapotranspiration from Temperature. *Appl. Eng. Agric.* **1985**, *1*, 96–99. [CrossRef]
68. QGIS. Development Team QGIS Geographic Information System. QGIS Association. *J. Open Source Softw.* **2021**, *6*. Available online: https://hub.qgis.org/ (accessed on 3 December 2025).
69. CONAGUA. *Actualización Hidrogeológica de Los Acuíferos: Maravatío-Contepec-Epitacio Huerta, Zacapu, Morelia-Queréndaro y Pastor Ortiz, en el Estado de Michoacán*; CONAGUA: Mexico City, Mexico, 2007.
70. Hu, S.; Ding, Y.; Cui, S.; Li, Y.; Zhao, J. Assessing Economic and Hydrological Effects of Water-Saving Irrigation Using a Coupled SWAT–MODFLOW–AquaCrop Model. *Agric. Water Manag.* **2025**, *314*, 109516. [CrossRef]
71. Zhang, J.; Zhang, M.; Song, Y.; Lai, Y. Hydrological Simulation of the Jialing River Basin Using the MIKE SHE Model in Changing Climate. *J. Water Clim. Change* **2021**, *12*, 2495–2514. [CrossRef]
72. Busico, G.; Ntona, M.M.; Carvalho, S.C.P.; Patrikaki, O.; Voudouris, K.; Kazakis, N. Simulating Future Groundwater Recharge in Coastal and Inland Catchments. *Water Resour. Manag.* **2021**, *35*, 3617–3632. [CrossRef]
73. Gashaw, T.; Dile, Y.T.; Worqlul, A.W.; Bantider, A.; Zeleke, G.; Bewket, W.; Alamirew, T. Evaluating the Effectiveness of Best Management Practices on Soil Erosion Reduction Using the Swat Model: For the Case of Gumara Watershed, Abbay (Upper Blue Nile) Basin. *Environ. Manag.* **2021**, *68*, 240–261. [CrossRef] [PubMed]
74. Kaur, S.; Chavan, S.R. Assessing the Impacts of Land Use and Climate Change on Streamflow Generation in the Nowrangpur Catchment Based on the SWAT–Land-Use Update Tool. *J. Water Clim. Change* **2025**, *16*, 70–91. [CrossRef]
75. Nepal, D.; Parajuli, P.B. Assessment of Best Management Practices on Hydrology and Sediment Yield at Watershed Scale in Mississippi Using SWAT. *Agriculture* **2022**, *12*, 518. [CrossRef]
76. Yang, X.; Dai, C.; Liu, G.; Li, C. Research on the Jiamusi Area's Shallow Groundwater Recharge Using Remote Sensing and the SWAT Model. *Appl. Sci.* **2024**, *14*, 7220. [CrossRef]
77. Hughes, J.D.; Russcher, M.J.; Langevin, C.D.; Morway, E.D.; McDonald, R.R. The MODFLOW Application Programming Interface for Simulation Control and Software Interoperability. *Environ. Model. Softw.* **2022**, *148*, 105257. [CrossRef]
78. Langevin, C.D.; Hughes, J.D.; Provost, A.M.; Russcher, M.J.; Panday, S. MODFLOW as a Configurable Multi-Model Hydrologic Simulator. *Groundwater* **2024**, *62*, 111–123. [CrossRef]
79. Nagaraj, S.; Masilamani, U.S. Simulation of Fluoride Transport in Groundwater Using Visual MODFLOW Flex and Human Health Risk Assessment. *Appl. Water Sci.* **2025**, *15*, 102. [CrossRef]

80. Choudhary, S.; Pingale, S.M.; Khare, D.; Krishan, R. Quantification of the Surface and Groundwater Dynamics of Upper Godavari Sub-Basin Using SWAT-MODFLOW and CMIP6 Climate Change Scenarios. *Hydrol. Sci. J.* **2025**, *70*, 1662–1685. [CrossRef]
81. Raja, O.; Parsinejad, M.; Tajrishy, M. Evaluation of Coupled SWAT-MODFLOW-NWT Model for Conjunctive Use of Surface Water and Groundwater Resources in the Mahabad Plain of Iran. *Sci. Rep.* **2024**, *14*, 32111. [CrossRef]
82. Carlos Mendoza, J.A.; Chavez Alcazar, T.A.; Zuñiga Medina, S.A. Calibration and Uncertainty Analysis for Modelling Runoff in the Tambo River Basin, Peru, Using Sequential Uncertainty Fitting Ver-2 (SUFI-2) Algorithm. *Air Soil Water Res.* **2021**, *14*, 1178622120988707. [CrossRef]
83. Harifidy, R.Z.; Hiroshi, I.; Kazuyoshi, S.; Jun, M.; Harivelo, R.Z.M.; Fernández-Palomino, C.A. Multi-Gauge Calibration Comparison for Simulating Streamflow across the Major River Basins in Madagascar: SWAT + Toolbox, R-SWAT, and SWAT + Editor Hard Calibration. *Hydrol. Res.* **2024**, *55*, 412–430. [CrossRef]
84. Khalil, K.; Khan, Q.; Mohamed, M. Modeling Aquifer Storage and Recovery in the Eastern District of the United Arab Emirates Using MODFLOW. *Sci. Rep.* **2022**, *12*, 17537. [CrossRef]
85. Saavedra, J.T.; Rosales, L.A.; Saavedra, O.C. Modelación de aguas subterráneas del valle de Cochabamba utilizando MODFLOW. *Investig. Desarro.* **2020**, *20*, 81–88. [CrossRef]
86. Mendoza, M.E.; Bocco, G.; Bravo, M.; Granados, E.L.; Osterkamp, W.R. Predicting Water-Surface Fluctuation of Continental Lakes: A RS and GIS Based Approach in Central Mexico. *Water Resour. Manag.* **2006**, *20*, 291–311. [CrossRef]
87. García Tinoco, M. Sequía Arrasó 70% del Lago de Cuitzeo en Michoacán. Available online: https://www.excelsior.com.mx/nacional/sequia-arraso-70-del-lago-de-cuitzeo-en-michoacan/1637140 (accessed on 14 July 2025).
88. Hernández-Bedolla, J.; Solera, A.; Paredes-Arquiola, J.; Pedro-Monzonís, M.; Andreu, J.; Sánchez-Quispe, S. The Assessment of Sustainability Indexes and Climate Change Impacts on Integrated Water Resource Management. *Water* **2017**, *9*, 213. [CrossRef]
89. Mendoza, M.E.; Granados, E.L.; Geneletti, D.; Pérez-Salicrup, D.R.; Salinas, V. Analysing Land Cover and Land Use Change Processes at Watershed Level: A Multitemporal Study in the Lake Cuitzeo Watershed, Mexico (1975–2003). *Appl. Geogr.* **2011**, *31*, 237–250. [CrossRef]
90. Correa-González, A.; Hernández-Bedolla, J.; Martínez-Cinco, M.A.; Sánchez-Quispe, S.T.; Hernández-Hernández, M.A. Assessment of Nitrate in Groundwater from Diffuse Sources Considering Spatiotemporal Patterns of Hydrological Systems Using a Coupled SWAT/MODFLOW/MT3DMS Model. *Hydrology* **2023**, *10*, 209. [CrossRef]
91. Navarro-Farfán, M.d.M.; García-Romero, L.; Martínez-Cinco, M.A.; Hernández-Hernández, M.A.; Sánchez-Quispe, S.T. Comparison between MODFLOW Groundwater Modeling with Traditional and Distributed Recharge. *Hydrology* **2024**, *11*, 9. [CrossRef]
92. Shinde, S.P.; Barai, V.N.; Al-Ansari, N.; Gavit, B.K.; Kadam, S.A.; Atre, A.A.; Bansod, R.D.; Elbeltagi, A. Characterization of Basaltic Rock Aquifer Parameters Using Hydraulic Parameters, Theis's Method and Aquifer Test Software in the Hard Rock Area of Buchakewadi Watershed Maharashtra, India. *Appl. Water Sci.* **2022**, *12*, 206. [CrossRef]
93. Moriasi, D.N.; Wilson, B.N.; Douglas-Mankin, K.R.; Arnold, J.G.; Gowda, P.H. Hydrologic and Water Quality Models: Use, Calibration, and Validation. *Trans. ASABE* **2012**, *55*, 1241–1247. [CrossRef]
94. Zhang, Y.; Chang, G.; Huang, B.; Xu, W.; Zhang, Z.; Liu, Z.; Zhang, S.; Ye, Z. Study on Mountains-Rivers-Forests-Farmlands-Lakes-Grasslands Measures of Reducing Nitrogen Load in the Upstream Watershed of North Canal Based on SWAT Model. *Huanjing Kexue Xuebao/Acta Sci. Circumstantiae* **2022**, *42*, 13–22. [CrossRef]
95. Nogueira, M.P.; da Silva, P.R.; Minoti, R.T. Influence of the Integrity of the Riparian Zone on the Capão Comprido Stream Water Basin (DF) by Simulating Different Spatial Discretizations with the SWAT+ Model. *Rev. Bras. Cienc. Ambient.* **2024**, *59*, e1743. [CrossRef]
96. Mahmoudpour, M.; Khamehchiyan, M.; Nikudel, M.R.; Ghassemi, M.R. Numerical Simulation and Prediction of Regional Land Subsidence Caused by Groundwater Exploitation in the Southwest Plain of Tehran, Iran. *Eng. Geol.* **2016**, *201*, 6–28. [CrossRef]
97. Almuhaylan, M.R.; Ghumman, A.R.; Al-Salamah, I.S.; Ahmad, A.; Ghazaw, Y.M.; Haider, H.; Shafiquzzaman, M. Evaluating the Impacts of Pumping on Aquifer Depletion in Arid Regions Using MODFLOW, ANFIS and ANN. *Water* **2020**, *12*, 2297. [CrossRef]
98. Elhakeem, M.; Papanicolaou, A.N. Evaluation of the Reduction in the Water Storage Capacity of Black Lake, AK. *Int. J. River Basin Manag.* **2008**, *6*, 63–77. [CrossRef]
99. Hosseini-Moghari, S.-M.; Araghinejad, S.; Tourian, M.J.; Ebrahimi, K.; Döll, P. Quantifying the Impacts of Human Water Use and Climate Variations on Recent Drying of Lake Urmia Basin: The Value of Different Sets of Spaceborne and in Situ Data for Calibrating a Global Hydrological Model. *Hydrol. Earth Syst. Sci.* **2020**, *24*, 1939–1956. [CrossRef]
100. Sacks, L.A.; Lee, T.M.; Swancar, A. The Suitability of a Simplified Isotope-Balance Approach to Quantify Transient Groundwater-Lake Interactions over a Decade with Climatic Extremes. *J. Hydrol.* **2014**, *519*, 3042–3053. [CrossRef]
101. Mahmoodi, N.; Hwang, H.T.; Struck, U.; Schneider, M.; Merz, C. Reinforce Lake Water Balance Component Estimations by Integrating Water Isotope Compositions with a Hydrological Model. *Hydrol. Earth Syst. Sci.* **2025**, *29*, 3993–4014. [CrossRef]


**Disclaimer/Publisher's Note:** The statements, opinions and data contained in all publications are solely those of the individual author(s) and contributor(s) and not of MDPI and/or the editor(s). MDPI and/or the editor(s) disclaim responsibility for any injury to people or property resulting from any ideas, methods, instructions or products referred to in the content.